ORIGINAL RESEARCH **Open access**

Dynamic Optimization of Electric Vehicle Charging Station Operations Using Multi-Parameter Scheduling

Andrew Miller[1*], Jessica Davis[1], Daniel Carter[2], Michael Lee[3]

Abstract

To enhance the convenience of charging electric vehicles (EVs), service providers are deploying extensive networks of charging stations (CSs). Current approaches address the dual goals of reducing costs and increasing profits for these providers through various avenues, including optimizing CS placement and refining pricing models. This research introduces a dynamic scheduling framework grounded in multiple parameters that incorporates energy management for CSs, integrating both energy administration and EV charging scheduling (EVCS). Furthermore, a comprehensive battery management system is developed specifically for energy storage purposes. We also present an advanced multi-parameter optimization algorithm, which features a CS selection operator designed around an alternative set and fine-tuned parameters. Experimental results demonstrate that the algorithms proposed herein achieve superior performance regarding optimization efficacy, iteration count, and overall stability.

Keywords Optimisation, Scheduling, Stability, Battery management system, Vehicle routing

*Correspondence:
Andrew Miller
andrew.miller@gatech.edu
[1] Department of AI for Resilient Power Systems, College of Engineering, Georgia Institute of Technology, Atlanta, United States
[2] Department of Intelligent Energy Informatics and Machine Learning, College of Engineering, University of Michigan, Ann Arbor, United States
[3] Department of Smart Grid Machine Learning, Faculty of Engineering, McGill University, Montreal, Canada

Introduction

Electric vehicles (EVs) have gained immense popularity recently, primarily due to their economic advantages [1]. To facilitate seamless charging experiences for EV owners, charging station (CS) service providers are deploying a vast number of CSs. Consequently, a persistent challenge for these providers is finding ways to minimize operational expenses while maximizing income. We frame this dual objective of cost reduction and revenue enhancement as a systemic issue, examining it through the lenses of energy management and electric vehicle charging scheduling (EVCS) to mitigate the challenges.

Regarding energy management, declining energy storage costs combined with time-of-use electricity pricing render effective energy control both feasible and appealing. As the battery sector evolves, the production expenses associated with energy storage batteries continue to drop while their storage capacities expand. Consequently, storing energy has become more economical. When paired with regional time-of-use pricing structures, mitigating power costs via energy storage emerges as a viable and lucrative strategy, particularly for CSs situated in urban centers. To implement this energy management, CS providers require a high-capacity battery energy storage system (BESS) for electricity retention. To attain the necessary high voltages and robust currents, it is standard practice to connect numerous battery cells in both series and parallel configurations [2, 3]. Currently, most commercial power batteries are constructed from lithium-

This is an open access article distributed under the terms of the Creative Commons Attribution-NonCommercial-ShareAlike 4.0 International License (CC BY-NC-SA 4.0), which permits non-commercial use, distribution, reproduction, and adaptation in any medium or format, provided that appropriate credit is given to the original author(s) and source, a link to the license is provided, and any changes made are indicated. Adapted material must be distributed under the same license.

© 2025 The Author(s). | Published by Institute of Smart Energy Systems Press

based compounds [4]. Inherent manufacturing variations among individual battery cells lead to widening voltage discrepancies during operation, making voltage inconsistencies increasingly pronounced. Therefore, a battery management system (BMS) is indispensable for overseeing the operational conditions of the battery framework and delivering a comprehensive suite of functions. In designing a BMS, numerous parameters must be evaluated. Techniques for assessing the state of charge (SoC) and state of health (SoH) remain primary focal points for investigators [5, 6].

Regarding battery equalization, hybrid balancing techniques have been introduced to accomplish cell balancing with greater efficacy [7, 8]. Within the structural architecture of the BMS, wireless battery management system (WBMS) frameworks have garnered increased focus [9]. Contemporary efforts in network scheduling aim to resolve congestion issues within WBMS environments [10]. Additionally, a digital twin framework for battery systems has been introduced to facilitate real-time monitoring and state estimation [11]. Ongoing investigations into network robustness are anticipated to enhance the operational capabilities of digital twin infrastructures [12-15]. In practice, a BMS is highly tailored, with varying operational contexts dictating distinct system requirements. Typical use cases include EVs [16, 17], electric motorcycles [18], aircraft [19], and autonomous underwater vehicles [20], most of which represent low-capacity implementations. Conversely, BESS technologies are already deployed on the utility grid side [21]. Currently, numerous BESS investigations prioritize the economic optimization of system operations [22].

To boost profitability and ensure business stability, CS service providers are open to forming commercial partnerships with EV ride-hailing enterprises. Consequently, CS providers need to collaborate with these hailing firms to develop comprehensive charging scheduling strategies for their fleets. Typically, the methodology for analyzing and resolving EVCS challenges involves three distinct phases. Initially, a charging scheduling framework that incorporates practical constraints must be formulated. Subsequently, various variables must be integrated to define a logical optimization objective. Ultimately, investigators apply an algorithmic approach to resolve the EVCS dilemma. An extensive body of research exists that explores diverse practical scenarios and corresponding algorithmic solutions. In situations where EV concentration is elevated during peak hours, vehicles are permitted to draw only enough power to reach their final destinations. To address this specific circumstance, Ref. [23] introduced an innovative genetic algorithm framework. To ensure that EVs consistently follow routes that optimize both power consumption and overall travel duration, Ref. [24] proposed a graph-oriented multi-objective heuristic approach. To minimize the aggregate charging duration of EVs while simultaneously shortening the distance between origin and destination, Ref. [25] suggested using a deep reinforcement learning model. Furthermore, Ref. [26] examined the EVCS challenge through the lens of EV ride-hailing businesses, advancing a mixed-variable differential evolution (MVDE) algorithm to manage the charging scheduling dilemma.

Based on the preceding literature review, several challenges persist. Firstly, concerning the BMS, while numerous investigations target the development of specific features—such as SoC calculation, SoH evaluation, and balancing mechanisms—there remains a notable deficiency in comprehensive, fully functional BMS solutions tailored for high-capacity BESS setups. Secondly, regarding the EVCS challenge, disparate research initiatives have employed varying premises and scheduling methodologies. Certain studies have tackled the EVCS issue from the standpoint of EV ride-hailing organizations [26]. However, evaluations of contemporary scheduling algorithms remain inadequate, and the operational stability of these algorithms in real-world applications has largely been overlooked. Furthermore, existing charging scheduling algorithms still require further optimization.

To address these limitations, we architect a comprehensive BMS and enhance an established charging scheduling algorithm. This manuscript maintains an application-centric focus, presenting the following principal contributions:

· To address the energy administration requirements of CS providers, we engineer and deploy a BMS specifically for large-capacity BESS environments. This BMS incorporates a suite of features that deliver comprehensive lifecycle battery administration capabilities.

· To delineate the practical utility of the scheduling algorithm, we evaluate three critical dimensions: optimization efficacy, convergence iteration count, and system stability. Furthermore, this study introduces a dedicated variance-

© 2025 The Author(s). | Published by Institute of Smart Energy Systems Press

centric methodology for assessing stability.

· Building upon the foundational MVDE algorithm, this research introduces a CS selection operator grounded in an alternative set and carefully calibrates the variables of the multi-parameter optimization framework. Findings indicate a substantial enhancement in the practical application of the baseline MVDE algorithm.

Related Work

BMS design

The architectural framework of a BMS is intrinsically tied to its intended operational context. Within the diverse categories of BMS applications, those engineered for EVs are characterized by their elevated voltage levels and expansive capacities. We categorize the functional capabilities of the BMS into three primary domains: data collection, system state computation and regulation, and system data communication. We have evaluated contemporary research advancements across these three domains, with the comparative findings detailed in **Table 1.**

Table 1. Comparison of recent research progress on battery management system (BMS)

Reference	Application	Data acquisition	System monitoring and control	Data management and communication
Cherukuri *et al*. [16]	Electric vehicle	Battery voltage measurements; temperature measurements; current measurements	Cell balancing control	SD card–based offline data storage; Linux-based graphical user interface
Chen *et al*. [18]	Electric motorcycles	Battery voltage measurements; temperature measurements; current measurements	Cell balancing control; battery protection management	Modular battery monitoring system
Tarhan *et al.* [19]	Aircraft	Battery voltage measurements; temperature measurements; current measurements	State-of-Charge (SoC) estimation; State-of-Health (SoH) estimation; cell balancing control; battery protection and management	User-oriented data transmission; offline data storage
Hu *et al*. [27]	Backup power system for communication base stations	Battery voltage measurements; temperature measurements; current measurements	State-of-Charge (SoC) estimation; cell balancing control; fault detection and diagnosis	Communication with the power and energy monitoring system

Targeting electric vehicle applications, Cherukuri *et al.* [16] engineered a battery management system tailored specifically to the high-voltage packs utilized in Formula Electric Racecars. While this setup captures fundamental metrics—such as

© 2025 The Author(s). | Published by Institute of Smart Energy Systems Press

current, temperature, and voltage—it only fulfills the elementary operational requirements of a BMS. In contrast to the architecture presented by Cherukuri *et al*., Chen *et al*. [18] developed a modular framework for electric motorcycles that offers expanded utility. Beyond gathering the three aforementioned parameters, their design actively operates the battery's protective switches, ensuring module safety during both charge and discharge cycles. Nevertheless, this configuration exhibits limitations, including a restricted scope of monitored variables and a lack of mechanisms to evaluate internal battery states.

Addressing power management hurdles within the aerospace sector, Tarhan *et al*. [19] formulated and deployed a hybrid BMS intended for aviation use. Their solution executes an array of tasks, from gathering diverse sensor readings and evaluating the pack's overall condition to actively regulating and safeguarding the energy cells. Furthermore, their proposed architecture accommodates the simultaneous management of two distinct battery chemistries. Investigating alternative lifecycles, Hu *et al*. [27] conceptualized an implementation strategy that repurposes decommissioned power batteries for backup energy at telecommunication base stations. They systematically engineered both the physical circuitry and the software stack, successfully enabling features like data acquisition, SoC projection, bus-based data exchange, active equalization, and error diagnostics.

Additionally, the station's primary power surveillance infrastructure interfaces directly with the BMS, facilitating seamless oversight and ongoing operational maintenance. Compared with the framework introduced by Tarhan *et al*. [19], this iteration offers a more comprehensive feature set, robust external communication capabilities, and greater real-world applicability. As illustrated in **Table 1**, contemporary academic efforts have achieved varying levels of functional maturity in BMS development.

Despite these advancements moving toward more sophisticated capabilities and accommodating larger storage reserves, the highlighted architectures remain unsuitable for massive-scale BESS deployments. Specifically, they suffer from limited parameter tracking and a narrow range of data exchange protocols. Furthermore, several of these models were never engineered for static energy storage. Consequently, we introduce a comprehensively equipped BMS tailored to this exact environment, refining multi-battery functional integration.

EVCS problem

Regarding the EVCS challenge, data from both vehicles and charging networks can be readily aggregated by infrastructure operators and ride-hailing firms to generate comprehensive scheduling strategies [28]. Their primary objective is to maximize systemic efficiency—specifically by slashing both temporal and financial expenditures associated with charging. Simultaneously, station administrators must account for the total electrical volume dispensed. While [29, 30] explored this exact dilemma, their methodologies rely heavily on analytical optimization techniques bounded by rigid theoretical assumptions. Given that the EVCS dilemma is formally classified as an NP-hard problem [1], leveraging evolutionary computation presents an ideal resolution strategy [31-33]. In particular, the Differential Evolution (DE) framework excels at the global optimization of continuous parameters [34].

Additionally, the deployment of both DE and Mixed-Variable Differential Evolution (MVDE) models has demonstrated substantial efficacy in prior literature [35-38]. Diverging from standard MVDE approaches, Liu *et al.* [26] structured the EVCS dilemma as a hierarchical optimization task, specifically factoring in the intrinsic correlations among the diverse variable types. Within this model, the fitness evaluation encompasses three critical dimensions: financial cost, temporal duration, and SoC levels. Subsequently, building upon conventional DE mechanisms, they introduced a novel MVDE paradigm. This included the engineering of several fresh evolutionary operators, namely a routing constructor for the CS, a hierarchical mixed-variable mutator, and a constraint-sensitive evaluator. These custom operators were specifically tailored to navigate the hierarchical complexities of the EVCS landscape, aiming for superior optimization trajectories. The researchers conducted an in-depth comparative analysis against competing frameworks. In defining their primary

© 2025 The Author(s). | Published by Institute of Smart Energy Systems Press

objectives, they anchored the algorithmic targets to the composite fitness metrics of time, cost, and SoC. Outcomes indicated that this MVDE approach outperformed alternative scheduling algorithms.

Nevertheless, limitations persist within their research. Specifically, their post-experiment analysis concentrated heavily on raw optimization gains, thereby neglecting a holistic appraisal of the algorithm's overarching operational performance. Furthermore, the speed at which the model iteratively converges requires further refinement. Consequently, our study enhances this baseline MVDE framework and conducts an exhaustive evaluation of its resulting capabilities.

System Structure and Operation Process

The overall structure of the system

Figure 1 illustrates the macroscopic architecture of the BESS. This energy storage setup consists of numerous battery packs dedicated to power retention, a high-current regulatory module, and the BMS. The core of the BMS is structured around a main control unit (MCU) alongside slave control units (SCUs), an arrangement exceptionally well-suited for high-capacity applications. To support peripheral operations, the BMS integrates supplementary components including a visual display, a data transmission interface, and a remote cloud server.

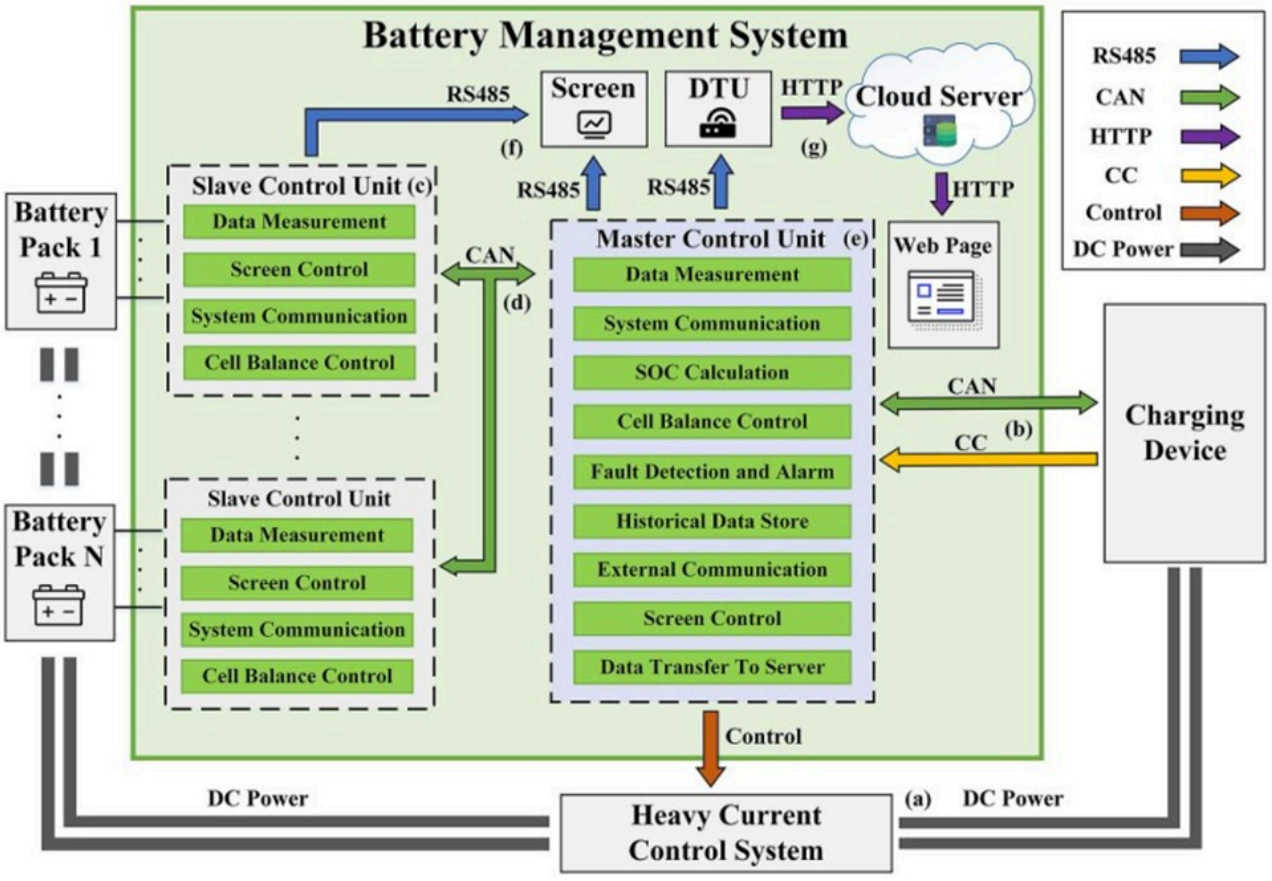

Figure 1. Battery energy storage system (BESS) block diagram.

Figure 1 outlines the constituent elements of the BESS. As charging or discharging occurs, power flows between external hardware and the battery clusters (Step (a)), a transfer strictly governed by the BMS (Step (b)). Within this management framework, the SCU executes various localized routines (Step (c)). Meanwhile, seamless internal data exchange between the MCU and the SCUs is facilitated via a Controller Area Network (CAN) bus (Step (d)). Simultaneously, the MCU

© 2025 The Author(s). | Published by Institute of Smart Energy Systems Press

processes a series of high-level tasks to enforce active regulation and state observation over the entire battery array (Step (e)). Output metrics are subsequently rendered on the local display (Step (f)) and uploaded to the centralized cloud infrastructure (Step (g)).

This manuscript details the comprehensive end-to-end development of the BMS, spanning both physical circuit fabrication and embedded software engineering. The STM32F413 microcontroller was chosen to drive both the MCU and the SCUs. The setup is supplemented by a diverse array of specialized functional modules and integrated circuits. Schematic drafting and printed circuit board routing for both units were executed using Altium software. On the software front, the BMS leverages the FreeRTOS real-time operating environment to orchestrate and execute its complex feature set.

The operation process of the system

During active operation, distinct categories of telemetry are gathered independently by the MCU and its subordinate SCUs. To centralize this information, the MCU commands the SCUs to transmit their localized readings upstream. Subsequently, by integrating real-time current and voltage metrics with the historical state parameters recorded during the previous cycle, the MCU computes and logs the updated SoC state value. Applying preconfigured balancing strategies, the MCU evaluates if the battery array requires cell equalization. If deemed necessary, the SCU is tasked with executing and overseeing the specific equalization routines.

Furthermore, the MCU continuously cross-references the system's operational health against predefined fault thresholds. Upon detecting an anomaly, it triggers appropriate warnings and executes corrective protocols as dictated by the situation. This cyclical workflow underpins the comprehensive battery management operation.

For local visualization, the MCU dictates a cyclical data push from the SCUs directly to the display terminal. In parallel, overarching system health metrics are broadcast to the cloud server. This remote repository archives the telemetry, serving it to end-users upon receiving web-based inquiries. Regarding charge and discharge regulation, the MCU continuously monitors the hardware handshake signals. Once a physical connection to an external charging apparatus is verified, the MCU commands the device to dictate power transfer based on the battery's real-time internal conditions.

System Function Design and Implementation

The architecture detailed in this study encompasses a diverse array of features, including battery voltage acquisition, internal state computation, and user interface rendering. These discrete capabilities synergize to enable the holistic operation of the BMS. The specific methodologies used to engineer and deploy these functions are outlined below.

Data collection

Battery voltage and temperature data collection

To capture thermal and voltage telemetry, the design incorporates the LTC6804 chip manufactured by Linear Inc. **Figure 2** delineates the electrical schematic of this module integrated within the SCU framework. To optimize spatial efficiency, a cluster of four LTC6804 units is embedded into every SCU. This allows a single SCU to simultaneously monitor up to 12 distinct temperature nodes and 48 cell voltages. Furthermore, to mitigate failure risks and simplify the architectural footprint, these chips are networked and communicate via a parallel topology.

© 2025 The Author(s). | Published by Institute of Smart Energy Systems Press

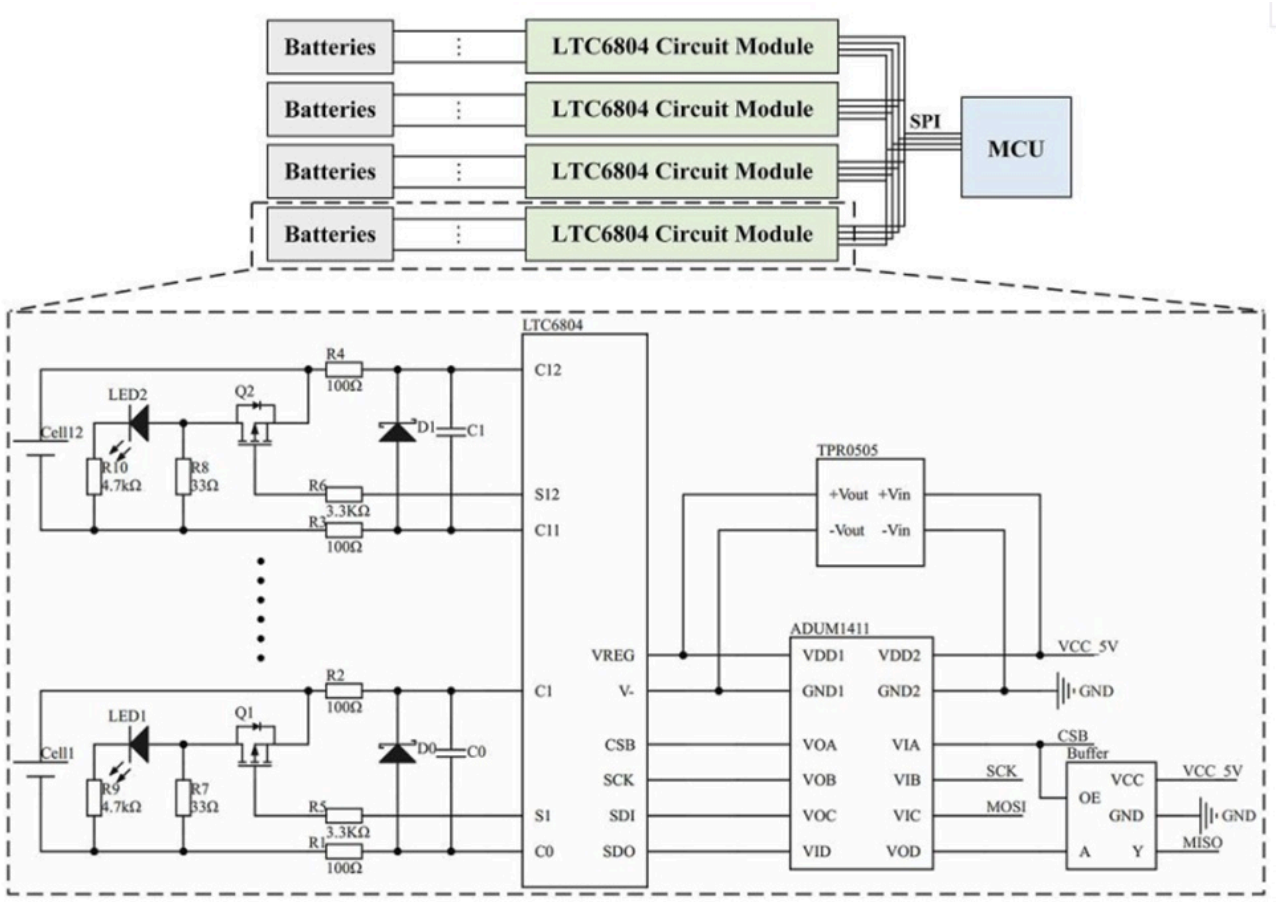

Figure 2. LTC6804 chip module circuit connection diagram.

Because the operational reference voltages fluctuate across the various LTC6804 modules within the SCU, robust electrical isolation is a critical design mandate. Consequently, the architecture utilizes a dedicated isolated power converter to energize the sensing chips, alongside digital isolators for the communication bus. Additionally, tri-state logic buffers are integrated to prevent signal collisions across the shared parallel lines.

Current data collection

Operating strictly via direct current for power cycling, the BMS captures amperage readings utilizing an integrated electricity metre paired with a resistive shunt. The metre extrapolates the flowing current by assessing the voltage drop across the shunt, and can be programmatically configured to track cumulative electrical usage.

High voltage data collection

For monitoring elevated voltage lines, the acquisition circuitry relies on a high-accuracy resistor divider network. This scales the severe potentials down to safe, low-voltage thresholds, which are subsequently quantified by a high-resolution analogue-to-digital conversion chip.

© 2025 The Author(s). | Published by Institute of Smart Energy Systems Press

Insulation state data collection

Diagnostic data regarding electrical isolation integrity is continuously acquired via a dedicated insulation surveillance module.

Smoke data collection

Environmental safety is maintained using a specialized sensor that detects ambient smoke. By registering fluctuating analog voltages that correlate with varying airborne gas concentrations, the system accurately gauges smoke levels.

System state calculation and control

SoC state calculation

Estimating the SoC relies on a hybrid methodology involving current integration paired with periodic battery baseline recalibration. Once the hardware remains idle beyond a defined temporal threshold, it automatically updates and archives the SoC data using the factory-provided chemical profiles. During active use, the architecture dynamically computes and stores the updated SoC by continuously monitoring the interplay between instantaneous current and battery voltage. **Eq. 1** details the mathematical formulation utilized for this SoC tracking:

$$SoC(t_n) = SoC(t_{n-1}) - \frac{\eta \cdot \Delta i \cdot \Delta t}{C_N} \quad (1)$$

Here, $SoC(t_n)$ denotes the charge status at a specific moment t_n, whereas $SoC(t_{n-1})$ reflects the measurement at the prior timestamp t_{n-1}. Additionally, η corresponds to the Coulombic efficiency factor, Δi captures the electrical flow difference across the temporal gap, Δt represents the duration of that interval, and C_N stands for the designated nominal capacity of the entire battery cluster. To compensate for thermal fluctuations affecting internal chemistry, the framework dynamically modifies C_N utilizing real-world temperature readings cross-referenced against manufacturer data.

During an active charge cycle, reaching the predefined full-charge voltage threshold triggers an automatic halt to power delivery, concurrently forcing the SoC calibration strictly to 100%. Conversely, when the cell voltages bottom out at the absolute 0% discharge limit during power draw, the system severs the load connection and zeroes out the SoC metric.

Battery balance

To mitigate severe voltage drift across individual cells, engineering an effective balancing mechanism is a mandatory component of BMS architecture. By leveraging the inherent discharge control capabilities of the LTC6804 integrated circuits, this architecture implements and regulates a passive equalization topology. Operationally, the balancing duties are structurally bifurcated between the SCU and the MCU. **Figure 3a** graphically illustrates this coordinated workflow.

© 2025 The Author(s). | Published by Institute of Smart Energy Systems Press

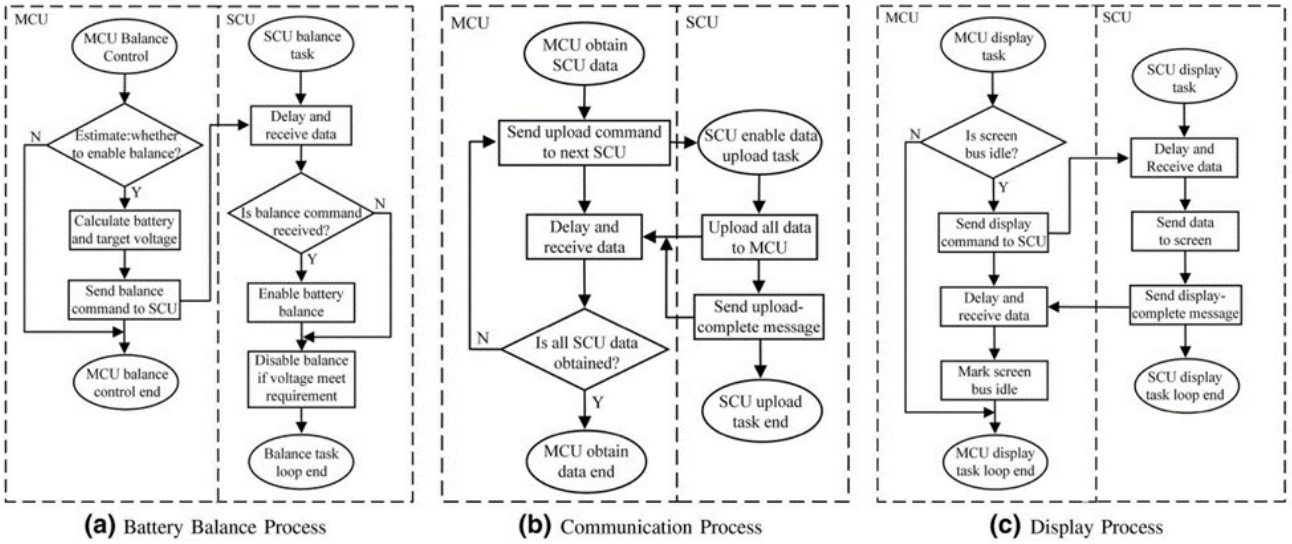

Figure 3. Flow chart of the BMS.

While active, the MCU continuously tracks inter-cell deviations, triggering the passive equalization protocols the moment maximum voltage deltas breach pre-programmed limits. Upon activation, the MCU identifies the specific cells exhibiting peak potentials—capped at a designated operational number—and computes the target step-down voltage required to resolve the imbalance based on a specified difference threshold. It then dispatches precise execution commands to the relevant SCU hardware. Upon receiving these directives, the assigned SCU engages the discharge circuit, actively managing and monitoring the cell-level equalization process.

Fault detection

To ensure holistic operational safety, the infrastructure sequentially scans for a wide spectrum of systemic anomalies to implement the fault detection function. Guided by configured safety logic, real-time telemetry is continuously compared against rigid diagnostic thresholds to determine whether failures have materialized, instantly classifying identified faults into prioritized severity tiers.

System data interaction

Internal communication

The BMS utilizes a CAN bus to establish connections between all MCU and SCU components. As most internal data flow involves the SCUs transmitting information to the MCU, the internal communication framework is structured as a command-execute model, reflecting the distinct functional roles of these units. The operational sequence for this communication function is detailed in **Figure 3b.**

The MCU periodically dispatches an upload command to the SCU to which it is currently tethered. Upon receiving this signal, the SCU immediately relays all current data and concludes with an upload-complete notification to the MCU. The MCU then issues the command to the subsequent SCU. This cycle repeats until the MCU has gathered all updated data. Furthermore, a limited number of supplementary commands and acknowledgment signals are exchanged throughout this internal communication routine.

© 2025 The Author(s). | Published by Institute of Smart Energy Systems Press

Historical data storage

By integrating a file system, the architecture enables read and write capabilities with a secure digital (SD) card, thereby facilitating the long-term archiving of historical system data.

Local display

The system employs a display screen to facilitate local data visualization. Each designated display field on the interface corresponds to a specific memory address. When refreshing metrics, the MCU or SCU transmits the data along with its designated address to the screen in the required format. Because of the substantial volume of BESS status metrics, prolonged screen update times can occur; consequently, the SCUs are configured to handle the transmission of the majority of this data. The operational workflow for this local display function is illustrated in **Figure 3c.**

During the display routine, the MCU issues a display command to the SCU, which then gains control of the bus and transmits data to the screen. To prevent interference, the MCU refrains from sending data while the bus is engaged. Once all SCUs have completed their data transmissions, the MCU resets the bus status to idle. The MCU retains overall control of the process, while the SCUs perform the bulk of the display operations.

Data remote access

System telemetry is relayed to the cloud server via a data transmission unit and archived in a database. Should the server receive a web-based request, it retrieves the relevant records from the database and transmits them to the client.

Charging process interaction

The system interfaces with external charging hardware via the CAN bus using standardized communication protocols, regulating the charging cycle based on the current state of the battery cluster.

Merits of BMS analysis

This section details the design and deployment of the proposed BMS across three functional domains: data acquisition, system state regulation and calculation, and data interaction. Regarding data acquisition, the BMS successfully gathers parameters such as battery voltage, current, insulation integrity, high-voltage status, and smoke detection, fulfilling the practical telemetry requirements for BESS. In the state calculation and control domain, we implemented SoC estimation, reduced inter-cell voltage disparities via passive balancing, and integrated fault detection to ensure systemic safety. Regarding data interaction, implementing distinct internal and external communication pathways enables users to monitor system status through various interfaces. Overall, the BMS delivers the essential functionalities required for BESS. Furthermore, the cell balancing, internal communication, and display routines have been independently optimized for compatibility with high-capacity BESS configurations. The inclusion of diverse data interaction modalities enhances the utility and operational practicality of the BMS.

EVCS Model

Basic assumptions

© 2025 The Author(s). | Published by Institute of Smart Energy Systems Press

The EVCS model represents the physical traffic network as a topology graph G(V, E), where V denotes the set of vertices and E denotes the set of edges.

The vertex set V corresponds to all intersections within the traffic network, while the edge set E represents the roadways connecting these intersections, with edge weights corresponding to road lengths.

In this model, continuous time is discretized into multiple time slots. A time slot defines the interval at which the scheduling algorithm updates the EV charging strategy. Consequently, the length of the time slot dictates the algorithm's operational frequency, impacting both response latency and computational demand. To optimize these parameters, the 24-hour day is divided into 96 time slots, each classified into one of three categories: peak, normal, or valley.

Each electric vehicle is defined as EV = (org, $d\ st$, t^{org}, β^{init}, β^{t}, r^{max}, *speed*), encompassing all variables relevant to the EVCS challenge. Here, org denotes the vehicle starting point, d st denotes the destination, and both org and d st are distinct vertices within the set $\boldsymbol{V}$. t^{org} represents the starting time slot, β^{init} represents the initial battery charge level at the start, β^{t} represents the charge level during the t - th time slot, β^{max} represents the maximum battery capacity, r^{max} denotes the vehicle's maximum driving range, and speed denotes the average travel velocity between the origin and destination. The SoC during the t - th time slot is determined by the ratio β^{t}/β^{max}.

Furthermore, this model assumes a direct proportional relationship between driving distance and energy consumption.

The traffic network contains several charging stations, with each CS situated along an edge. A charging station is defined as CS = {l, $y^{f,m}$, $y^{s,m}$, $\boldsymbol{p}^{f}$, $\boldsymbol{p}^{s}$ }. Here, l specifies the location of the CS within the network, $y^{f,m}$ and $y^{s,m}$ denote the maximum quantity of fast and slow chargers available at the station, respectively, and, $\boldsymbol{p}^{f}$ = {$p^{f,\text{valley}}$, $p^{f,\text{normal}}$, $p^{f,\text{peak}}$} and $\boldsymbol{p}^{s}$ = {$p^{s,\text{valley}}$, $p^{s,\text{normal}}$, $p^{s,\text{peak}}$} represent the charging tariffs for fast and slow chargers during valley, normal, and peak periods.

Problem formalisation

We employ the proposed multi-parameter optimization algorithm to address the EVCS problem. The specific algorithm is detailed in the subsequent section. The solution representation within this algorithm is illustrated in **Figure 4**. Each candidate solution S within the population is defined as $\boldsymbol{S}$ = { $\boldsymbol{s}_1$, $\boldsymbol{s}_2$, …, $\boldsymbol{s}_i$ }.

In this representation, S n denotes the aggregate solutions generated for all EVs, while s i denotes the individual schedule for EV i. The solution s i is expressed as $\boldsymbol{s}_i$ = [(cs_{i1}, o_{i1}, e_{i1}), …, (cs_{ij}, o_{ij}, e_{ij})], comprising a sequence of selected charging operations. Here, cs_{ij} represents the j - th charging station on the path chosen for EV_i , o_{ij} signifies the selected charging mode at that station, e_{ij} relates to the electrical energy charged at that station, and the triplet (cs_{ij}, o_{ij}, e_{ij}) constitutes a single charging operation for EV i.

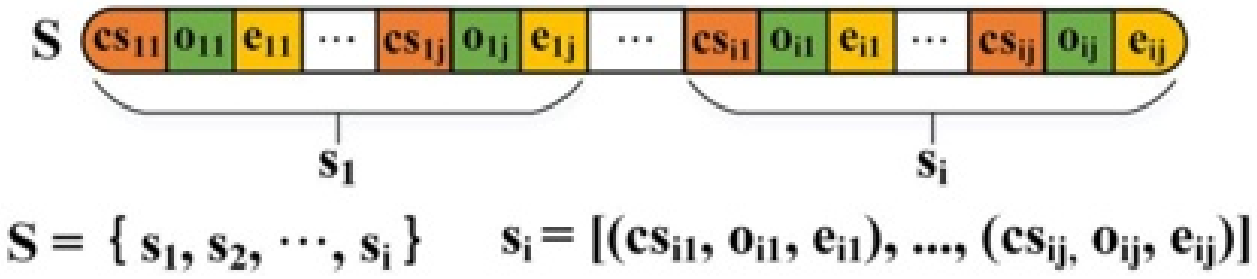

Figure 4. Solution structure of population.

© 2025 The Author(s). | Published by Institute of Smart Energy Systems Press

CS path: The sequence of multiple cs_{ij} involved in the various charging operations within s i forms the CS path chosen for EV i. Furthermore, the total quantity of CSs included in this path cannot exceed J. Consequently, this means the overall count of charging operations within s i is bounded by J. To determine the travel route between varying stations, a shortest path algorithm is applicable. Thus, selecting a CS path effectively establishes the EV's trajectory from its origin to its final destination. The CSs comprising the CS path must be distinct and accessible.

Charging option: The variable o ij denotes the specific charging method utilized by EV i at the j − th CS. Within this framework, two prevalent real-world charging techniques are incorporated: fast charging and slow charging. Consumers can select either a fast or slow charger. This choice directly influences both the duration and the financial expense of the charging process. To illustrate, fast chargers can fully replenish an EV's battery within 1–2 h, whereas slow chargers often require significantly more time. Furthermore, the financial rates associated with these distinct charging modes vary, even within the identical CS.

Extra charging rate: The parameter e ij dictates the volume of electricity supplied to EV i during its charging session at the j − th CS, bounded within the interval e i ∈ [0, 1]. Integrating this rate into the proposed solution helps in identifying the optimal amount of electricity needed for the EV. If we define the electricity replenished for EV i at the j − th CS as β_{ij}^{charge}, and the minimum energy necessary to reach the subsequent station as β_{ij}^{min}, then the extra charging rate for EV i at the j − th CS is formulated as follows:

$$e_{ij} = \frac{\beta_{ij}^{charge} - \beta_{ij}^{\min}}{\beta_{ij}^{\max} - \beta_{ij}^{\min}} \quad (2)$$

Fitness function: The evaluation of fitness incorporates three primary dimensions: time expenditure, charging expenses, and the battery's state of charge. The comprehensive fitness function integrates these three elements and is formulated as:

$$f(S) = \frac{f_{time}^{average}(S)}{f_{time}^{\max}} + \frac{f_{cost}^{average}(S)}{f_{cost}^{\max}} + \frac{f_{SoC}^{average}(S)}{f_{SoC}^{\max}} \quad (3)$$

In this context, S stands for the comprehensive solution produced by the scheduling algorithm across all participating EVs. The terms $f_{time}^{average}$(S), $f_{cost}^{average}$(S), and $f_{SoC}^{average}$(S) denote the solution's average time expenditure, average charging expense, and average SoC gap, respectively. Additionally, $\mathrm{f}_{\mathrm{time}}^{\max}$, $f_{cost}^{\max}$ and $f_{SoC}^{\max}$ represent the maximum possible values for time cost, charging expense, and SoC discrepancy.

Time cost: Time cost reflects the cumulative duration required for an EV driver to conclude the entire journey—encompassing travel and charging—from their initial location to their destination. This includes actual driving periods, active charging durations, and any potential queueing delays at the CS. For a given solution S, the average time expenditure is defined as:

$$f_{time}^{average}(S) = \frac{\sum_i \left(t_i^{dst} - t_i^{org}\right)}{n} \quad (4)$$

Here, where t_i^{dst} and t_i^{org} indicate the specific time slots during which EV i departs from its origin and reaches its final destination, according to the formulated scheduling plan. The maximum time cost $f_{time}^{average}$(S) is established as 96.

Charging cost: An EV's overall charging expense is computed as the aggregate of the financial costs incurred at every chosen CS. The upper limit for an EV's charging expenditure is evaluated as follows:

© 2025 The Author(s). | Published by Institute of Smart Energy Systems Press

$$f_{cost}^{\max} = \frac{\sum_i \left(J \times \beta_i^{\max} \times p_{avg}^{peak} \right)}{n} \quad (5)$$

In this equation, p_{avg}^{peak} signifies the mean charging tariff across all CSs during periods of peak demand, while $\beta_i^{\max}$ denotes the ultimate battery capacity of EV i. Furthermore, the average financial cost of charging is modeled as:

$$f_{cost}^{average}(S) = \frac{\sum_i \sum_j f_{cost}^{charge} \left(\beta_{i,j}^{charge}, p_{i,j} \right)}{n} \quad (6)$$

Herein, $\beta_{i;j}^{charge}$ characterizes the volume of electricity replenished for EVi at the chosen CSj, pi,j indicates the specific charging rate at that location, and $f_{cost}^{charge}(\cdot)$ denotes the resulting charging expense derived from both the consumed electricity and the prevailing price.

SoC gap: The SoC discrepancy is defined as the variance between the vehicle's state of charge upon arriving at its destination and the initially targeted SoC. This metric is computed as:

$$f_{SoC}^{i}(S) = \begin{cases} 1 - \rho_i^{des}, & \text{if } \rho_i^{des} < \rho^{\exp} \\ \rho_i^{des} - \rho^{\exp}, & \text{otherwise} \end{cases} \quad (7)$$

In this context, $\rho^{\exp}$ stands for the desired SoC threshold, whereas p_i^{des} signifies the actual SoC level when EV i arrives at its endpoint. Because both $\rho^{\exp}$ and p_i^{des} are confined to the interval [0, 1], the resulting calculation for $f_{SoC}^{i}(S)$ is guaranteed not to surpass 1. Consequently, the maximum allowable SoC gap is defined as $f_{SoC}^{\max} = 1$. To determine the average SoC discrepancy across the entire fleet of EVs, the following formula is applied:

$$f_{SoC}^{average}(S) = \frac{\sum_i f_{SoC}^{i}(S)}{n} \quad (8)$$

Where n corresponds to the total quantity of EVs.

Overall model

Building upon the previously detailed characteristics of the EVCS challenge, the problem framework can be mathematically formalized as follows:

$$min \quad f(S) \quad (9)$$

$$s.t. \quad |cs_i| \leq J \quad (10)$$

$$\beta_i^t / \beta_i^{max} \in [0, 1], \quad \forall t, \quad \forall i \quad (11)$$

© 2025 The Author(s). | Published by Institute of Smart Energy Systems Press

$$\sum_i f_{\text{status}}^{\text{charge}}(i,j,o,t) \le \gamma_j^{o,\max}, \quad \forall j, \quad \forall o, \quad \forall t \quad (12)$$

The fitness evaluation within the EVCS model comprehensively addresses several dimensions, including time expenditures, financial charging costs, and the SoC discrepancy. **Eq. 10** imposes a constraint on the total number of CSs allocated to an individual EV. In this expression, cs i is composed of the various cs ij elements within s i and is denoted as $\boldsymbol{cs}_i = [cs_{i1}, \ldots, cs_{ij}]$. For any given EV i, **Eq. 11** delineates the permissible boundaries of its SoC during the t − th time slot. Here, β_i^t refers to the energy level of EV i's battery at the t − th time slot, while β_i^max indicates EV i's peak battery capacity. Furthermore, **Eq. 12** states that during any given time slot, the number of EVs receiving a charge at CS j cannot exceed the maximum number of operational chargers at that site. The expression $\sum_i f_{cost}^{charge}(i, j, o, t)$ quantifies the aggregate number of EVs utilizing the o − th charging option at CS j during the t − th time slot.

The Multi-Parameters Optimisation Algorithm

Framework of multi-parameters optimisation algorithm

The complete operational workflow for EVCS is illustrated in **Figure 5**. This procedure is structurally partitioned into three distinct phases: data collection and preparation, the generation of the scheduling scheme, and the subsequent updating of this scheduling scheme. During the initial data preparation phase, the framework gathers comprehensive information concerning the transportation networks, operational CSs, and specific EVs requiring charging services. Following this, the scheduling scheme generation phase involves the algorithm formulating an optimal charging and routing plan for the entire fleet of EVs. The specific multi-parameter optimization algorithm implemented in this study encompasses several procedural operations. These include a CS selection mechanism derived from an alternative set, an MVDE mutation procedure, conventional crossover techniques, constraint-aware evaluations, and standard selection methodologies. Finally, within the scheduling scheme update phase, the newly formulated charging plan is broadcast to all corresponding EVs. This entire sequence operates iteratively to continuously satisfy the dynamic charging and scheduling requirements of the EVs.

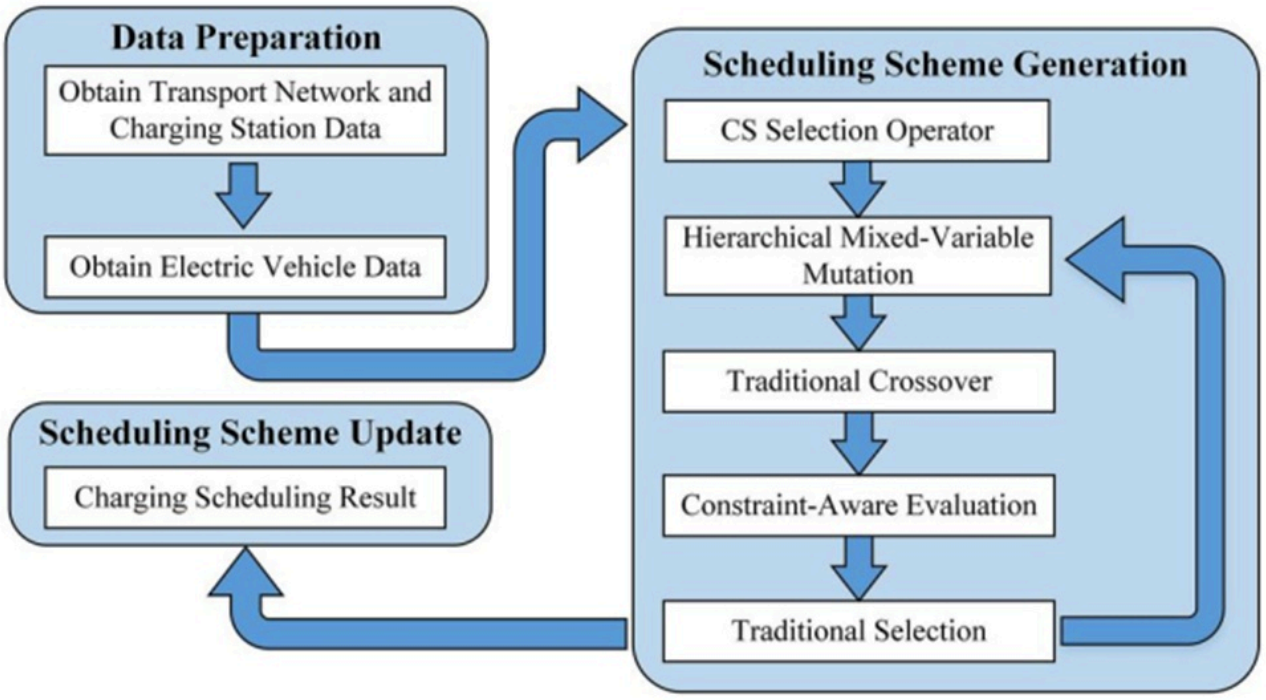

Figure 5. Overall process of electric vehicle charging scheduling (EVCS) algorithm.

© 2025 The Author(s). | Published by Institute of Smart Energy Systems Press

Throughout the generation phase of the scheduling scheme, this approach adheres to the MVDE algorithmic operators outlined in ref. [26], which includes implementing the hierarchical mixed-variable mutation operator alongside the constraint-aware evaluation technique. Similarly, the mechanisms utilized for crossover and selection directly mirror the conventional methods detailed in ref. [26]. The sole divergence from that existing framework occurs within the hierarchical mixed-variable mutation phase, wherein the randomized selection of CSs is strictly limited to the designated CS alternative set.

CS selection operator based on alternative set

During the creation of a scheduling plan, the MVDE algorithm identifies one or multiple CSs for an EV. Conventional CS selection operators typically choose several CSs from the complete pool of available stations within the entire traffic network, subsequently routing the EV from its origin to its destination. However, this approach risks exploring invalid search spaces. Restricting the selection process helps mitigate these invalid domains. Practically speaking, only a specific subset of CSs is logically viable and ought to be considered during the selection phase. The fundamental premise of the alternative set-based CS selection operator is to establish a designated CS alternative set for every EV during the initial phases of the MVDE algorithm. This established set is then systematically utilized across all subsequent CS selection procedures.

The primary criterion for defining the alternative set is guaranteeing that the linear distance between the EV and its final destination continuously decreases throughout the planned route. Guided by this principle, a circular boundary serves as the core component of the methodology for establishing the alternative set. The precise mechanics of this method are detailed as follows. As illustrated in **Figure 6**, the red and green dots denote the EV's origin and destination, respectively, while the black dot signifies the midpoint of the segment linking these two locations. Initially, to ensure that the EV's starting battery level is sufficient to reach at least one station, the alternative set incorporates the CSs located closest to the origin, exemplified by CS: A and CS: B in **Figure 6**. The specific value of o is derived from the parameter selection experiment. Subsequently, a circular boundary is constructed using the coordinates of the start and end points, where the line segment connecting them acts as the diameter. Any CS situated within or perfectly on the perimeter of this circle, such as CS: C and CS : D, is integrated into the alternative set. Conversely, stations positioned beyond the circular boundary, such as CS: E, are excluded.

By employing this alternative set methodology, every CS located within the circle fulfills the aforementioned criterion. The mathematical proof for this is outlined below, evaluating scenarios where the CS is positioned either inside or outside the defined circle. Referring to **Figure 7**, let S represent the EV's initial location and D signify its destination. For a scenario where the CS is located inside the circle, assuming C_1 is the chosen station, the resulting travel route is composed of SC_1 and $C_1 D$. The point R_1 represents the intersection between the circle and the extended line of SC1. Let K_{t1}, K_{t2}, and K_{t3} represent three chronologically sequential points along the EV's route, satisfying the condition: $t_1 < t_2 < t_3$. $K_{t1} D$, $K_{t2} D$, and $K_{t3} D$ denote the direct linear distances from these respective points to the final destination. Based on the geometry in **Figure 7**, the angles follow the relationship $\theta_1 < \theta_2 < \theta_3$, and the corresponding edges adhere to the formulas: $K_{t1} D = R_1 D/\sin\theta_1$, $K_{t2} D = R_1 D/\sin\theta_2$, and $C_1 D = R_1 D/\sin\theta_3$. Consequently, $K_{t1} D > K_{t2} D > K_{t3} D$. This mathematically demonstrates that the core criterion is upheld when the chosen CS is situated inside the circle. Conversely, if the CS lies outside the circle, let us assume $C2$ is the chosen station, making the travel route SC2 and C2D. The point R2 is where SC_2 intersects the circle boundary. Let K_{t4} and K_{t5} denote two sequential points along this route, adhering to the temporal relationship: $t_4 < t_5$. As shown in **Figure 7**, the angles relate as $\theta_4 > \theta_5$, and the lengths follow the relations: $K_{t4} D = R_2 D/\cos\theta_4$ and $K_{t5} D = R_2 D/\cos\theta_5$. Therefore, $K_{t4} D < K_{t5} D$. This clearly indicates that the requisite criterion fails when the chosen CS resides outside the circular boundary.

Utilizing the methodology detailed above allows for the identification of an appropriate CS alternative set tailored to each EV. Throughout the computational execution of the scheduling algorithm, all operations about CS selection are strictly confined to this defined alternative set, entirely bypassing the comprehensive pool of all network CSs.

© 2025 The Author(s). | Published by Institute of Smart Energy Systems Press

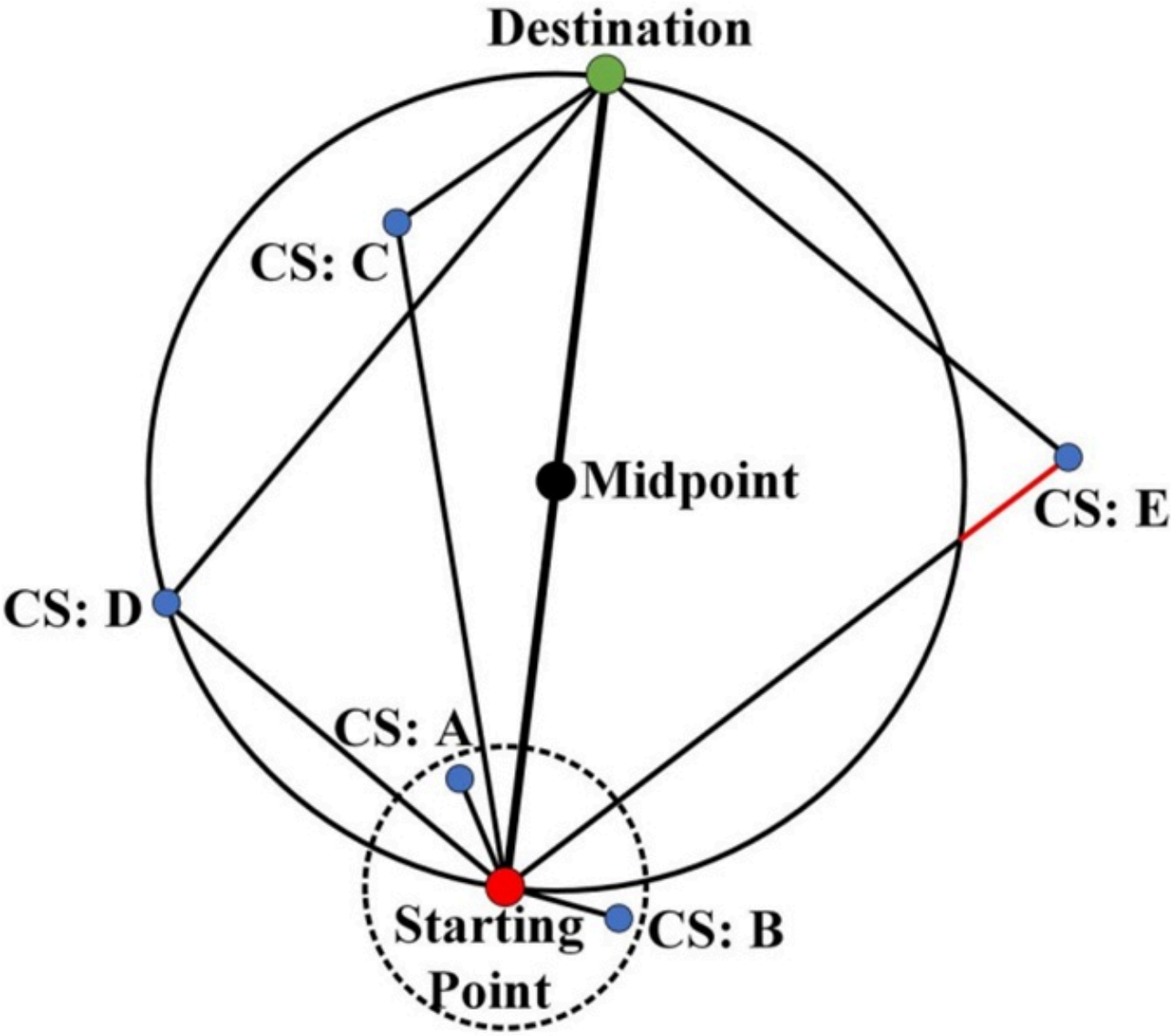

Figure 6. Example of alternative set setting method.

© 2025 The Author(s). | Published by Institute of Smart Energy Systems Press

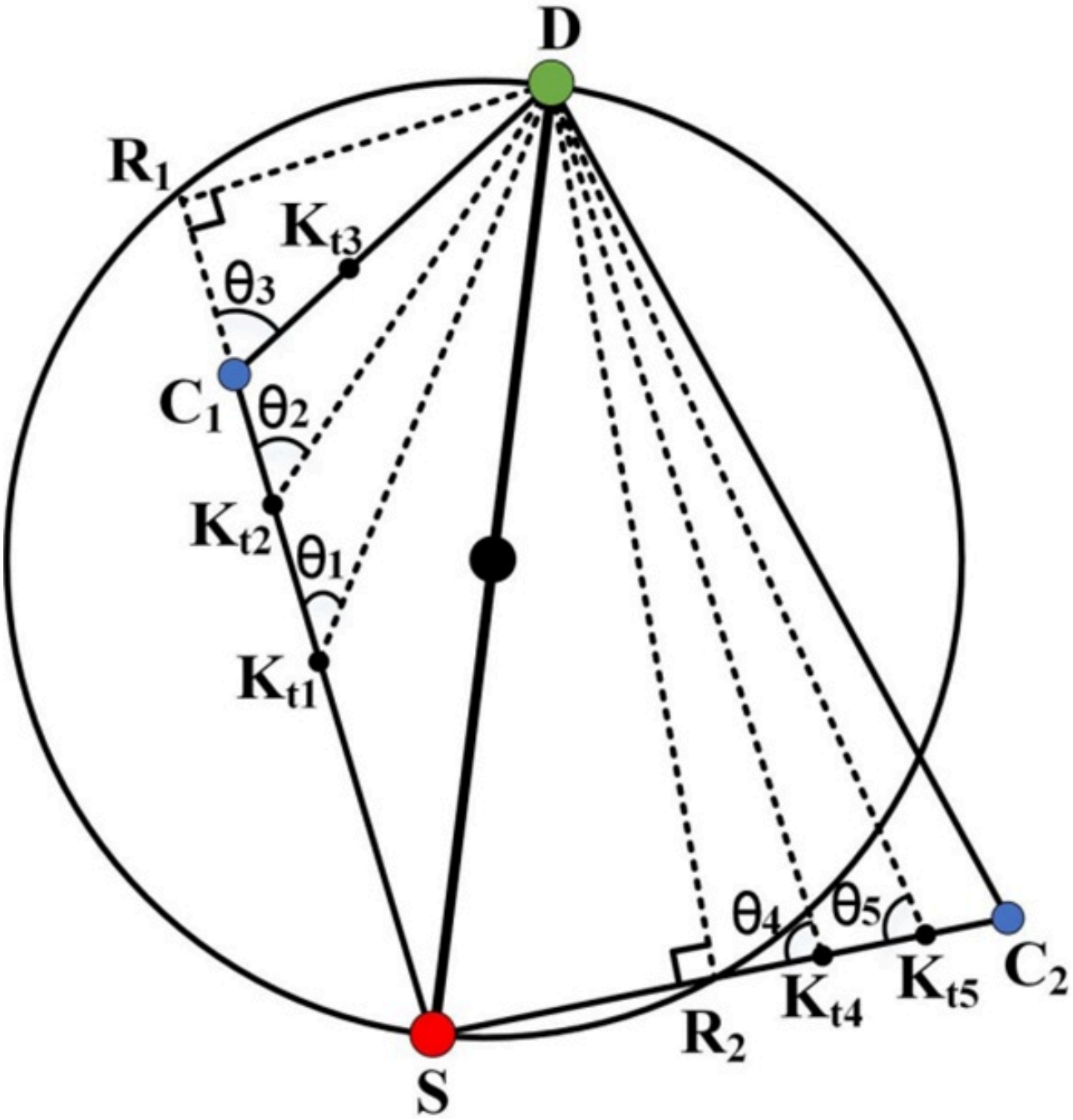

Figure 7. Proof of the criterion of alternative set method.

Stability evaluation method for evolutionary algorithm

The EVCS challenge is widely recognized as an NP-hard problem, meaning it is typically addressed utilizing global heuristic computational methods. In this study, for instance, a multi-parameter optimization algorithm is deployed to tackle the EVCS issue. A ubiquitous challenge when applying evolutionary algorithms is their inherent susceptibility to becoming trapped in local optima. Ideally, the outputs generated by the algorithm should be highly similar; this characteristic defines the stability of the evolutionary approach. More specifically, when the algorithm undergoes multiple, independent iterative

© 2025 The Author(s). | Published by Institute of Smart Energy Systems Press

trials, the resulting outcomes should align as closely as possible with the overall average result. This degree of outcome consistency directly reflects the algorithm's inherent stability.

Within the realm of probability theory, variance functions as a critical metric of dispersion, quantifying the spread between a given dataset and its corresponding mean value. To properly assess an evolutionary algorithm's stability, it is imperative to quantify the degree of discreteness existing between the discrete outcomes of repeated, independent trials and their collective average. Consequently, variance is adopted as the primary mathematical tool for evaluating the stability of the proposed evolutionary algorithm.

To systematically evaluate the stability of an evolutionary algorithm, the process begins by subjecting the algorithm to a series of independent, repeated experimental trials, all conducted under identically controlled conditions. Following this, the mean outcome across all these trials is computed. The specific threshold defining algorithmic convergence must be tailored to the exact nature of the problem at hand. Within the context of this study, convergence is acknowledged if the maximal deviation in the optimization outcome between a given generation and its 10 preceding generations falls below 0.005. The specific iteration count at which this average result achieves convergence is formally defined as $Iter^{conver}$. To mitigate the skewing impact of substantial variabilities present during the initial phases of the optimization sequence, the variance-based stability calculation focuses exclusively on the 50 iterations immediately before $Iter^{conver}$. As illustrated in **Figure 8**, the red trajectory depicts the mean optimization outcome, with the variance computation restricted solely to the final 50 generations.

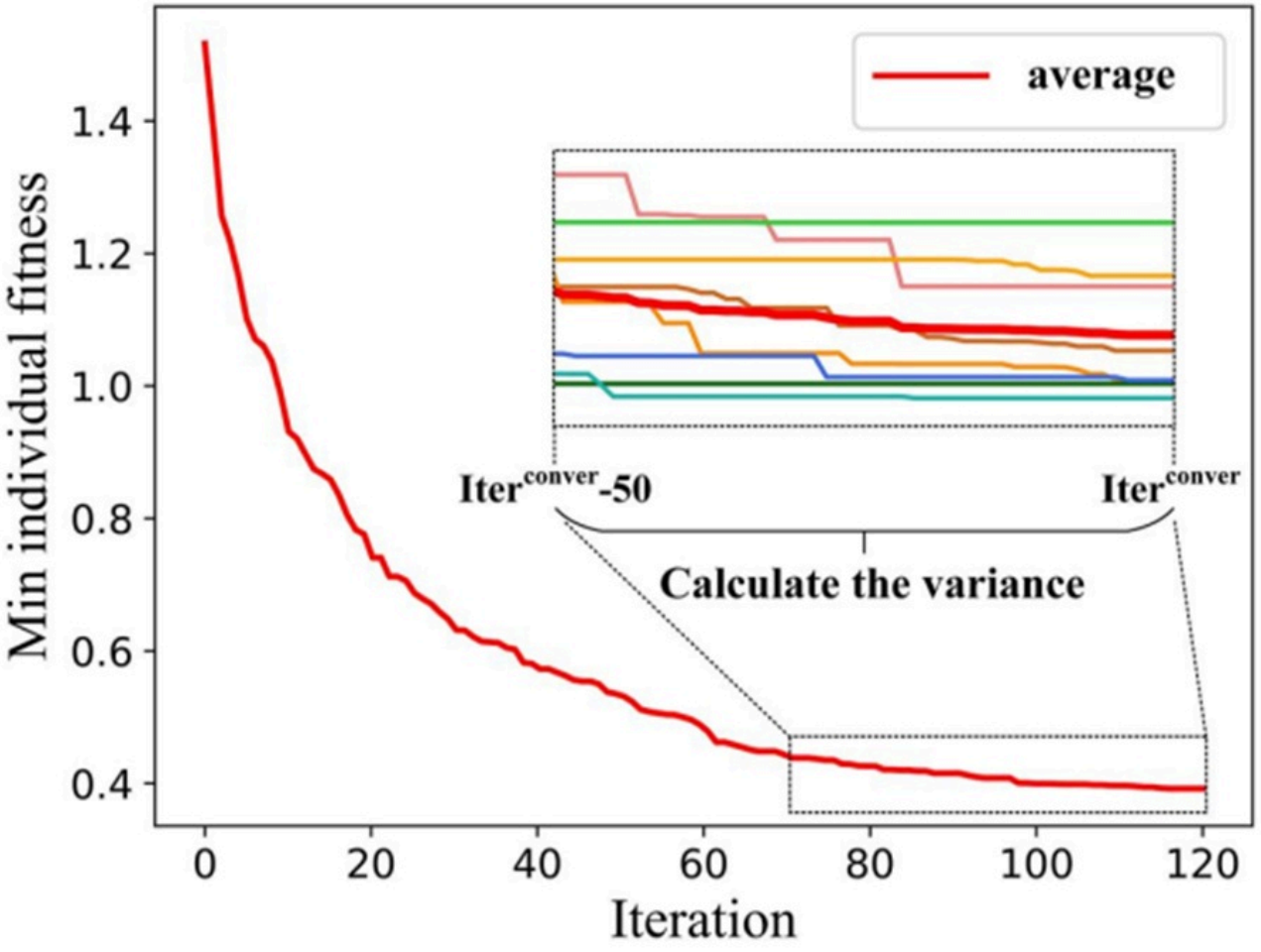

Figure 8. Example of stability calculation.

© 2025 The Author(s). | Published by Institute of Smart Energy Systems Press

The explicit formula for this calculation is articulated in **Eq. 13**:

$$S = \frac{\sum_{i=0}^{N} \sum_{j=Iter^{conver}-50}^{Iter^{conver}} \left(fitness_{ij} - fitness_{j}^{average} \right)^2}{N \times 50} \quad (13)$$

In this equation, S denotes the computed stability metric of the evolutionary algorithm, N corresponds to the total count of independent and repeated experimental trials, and *Iter* ^{conver} signifies the specific iteration index at which the mean outcome fulfills the convergence criteria. Furthermore, fitness ij signifies the calculated fitness metric for the j − th iteration during the i − th independent trial, while $fitness_j^{average}$ denotes the average fitness value documented at the j − th iteration.

Evolutionary algorithms often yield unstable optimization outputs due to their propensity to become ensnared in local optima. The introduced methodology for evaluating stability quantifies the discreteness of these optimization outcomes by executing the algorithmic sequence repeatedly under uniform conditions, ultimately deriving a comprehensive stability metric. When deploying this evaluative approach, conducting a higher volume of independent, repeated experiments yields significantly more robust stability metrics, effectively neutralizing measurement anomalies stemming from random chance. Naturally, more experimental iterations require longer testing durations. As a result, a calculated compromise between rigorous accuracy and temporal efficiency must be established when implementing this technique. Furthermore, the volume of constraints placed upon the optimization algorithm can directly influence its likelihood of stalling at a local optimum. In scenarios involving algorithms that are severely vulnerable to local optima entrapment, it is highly recommended to augment the number of independent trials to adequately suppress the influence of probabilistic chance.

Experiments

Experiments of battery management system

Within the system architecture, every SCU integrates four individual LTC6804 chips, each capable of concurrently monitoring the voltages across 12 series-connected batteries. The internal circuit module blueprint is identical across all four of these chips. Consequently, for this experimental evaluation, a single LTC6804 unit is employed to measure a string of 12 batteries linked in series. The specific energy cell utilized throughout this testing phase is an 18,650 lithium battery featuring a designated capacity of 2600 mAh.

Battery voltage data collection

An individual LTC6804 chip housed within the SCU can monitor the complete array of 12 batteries or a reduced subset. Operators can gather voltage data from a smaller cluster of batteries by adhering to the wiring configuration illustrated in **Figure 9.**

© 2025 The Author(s). | Published by Institute of Smart Energy Systems Press

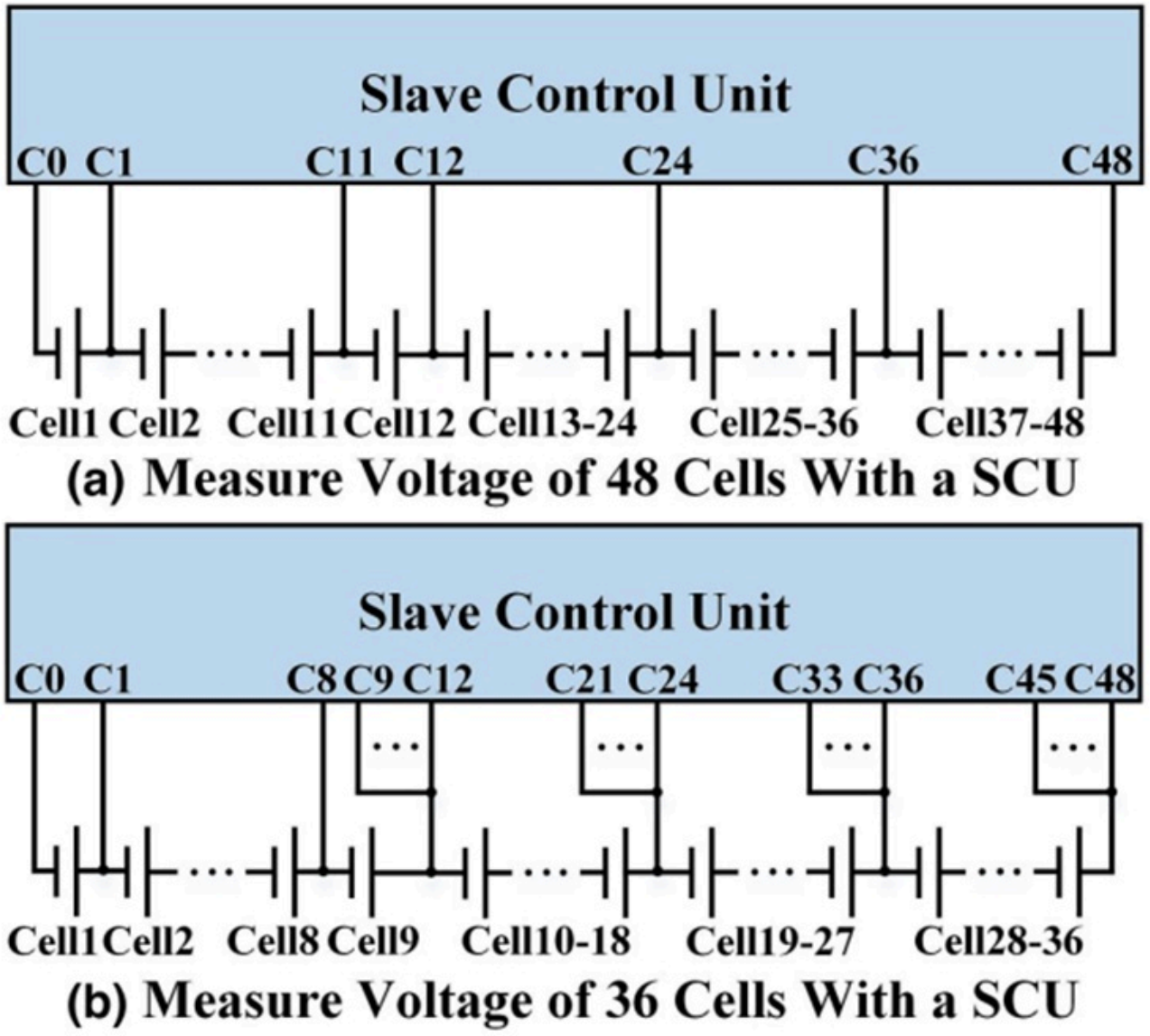

Figure 9. The connection method of different numbers of batteries.

Voltage readings are systematically gathered from the complete set of 12 batteries. To validate the system's operational capacity to monitor a restricted number of units, voltage data from a configuration of exactly nine batteries is similarly acquired. To establish an accurate reference baseline, a highly precise voltmeter is utilized to record the true voltage values. As evidenced by the empirical data presented in **Table 2**, the total measurement error incurred during battery voltage collection remains strictly under 2 mV.

Table 2. Battery voltage collection results

Number	Reference (V)	12 batteries collection		9 batteries collection	
		Voltage (V)	Error (mV)	Voltage (V)	Error (mV)
1	3.6872	3.6883	1.1	3.6883	1.1

© 2025 The Author(s). | Published by Institute of Smart Energy Systems Press

2	3.7937	3.7951	1.4	3.7951	1.4
3	3.7483	3.7496	1.3	3.7496	1.3
4	3.6551	3.6564	1.3	3.6563	1.2
5	3.5405	3.5417	1.2	3.5416	1.1
6	3.5545	3.5557	1.2	3.5556	1.1
7	3.6487	3.6494	0.7	3.6494	0.7
8	3.5636	3.5644	0.8	3.5643	0.7
9	3.7634	3.7642	0.8	3.7642	0.8
10	3.7820	3.7826	0.6	–	–
11	3.5771	3.5777	0.6	–	–
12	3.6614	3.6619	0.5	–	–

Battery balance

A passive balancing mechanism is employed to equalize the state of the individual batteries. Taking into account the thermal dissipation capabilities of the SCU, a 33 Ω power resistor was chosen to facilitate the active discharge of a specific battery. The resulting balancing current is approximately 100 mA, corresponding to a balancing discharge power of nearly 0.33 W. Systematically, the overarching framework is fully capable of simultaneously activating a maximum of six parallel balancing circuits.

The system's balancing feature was meticulously evaluated under two distinct operational states: a no-load scenario and an active discharge scenario. Within **Figure 10a** and **Figure 10c**, a representative sample of five batteries was selected via interval numbering to analytically depict the comprehensive status of the entire 12-battery array. Specifically, **Figure 10a** illustrates the fluctuations in battery voltage once the balancing operation is initiated in an unloaded environment. Conversely, **Figure 10b** tracks the corresponding trajectory of the peak voltage discrepancy during this same no-load phase. Analytical findings reveal that it took 100 min to reduce the maximum voltage divergence from 0.1026 V to 0.0098 V. Transitioning to active loads, **Figure 10c** visualizes the battery voltage adjustments triggered by the balancing sequence during an ongoing discharge event. **Figure 10d** concurrently charts the progression of the maximum voltage disparity during this discharge phase. The experimental outcomes demonstrate a sharp decline in the maximum voltage gap throughout the initial 50 min of discharging, after which it plateaus at approximately 0.065 V. This stabilization occurs because the active balancing effect fundamentally counteracts the voltage divergence inherently exacerbated by the discharging process.

© 2025 The Author(s). | Published by Institute of Smart Energy Systems Press

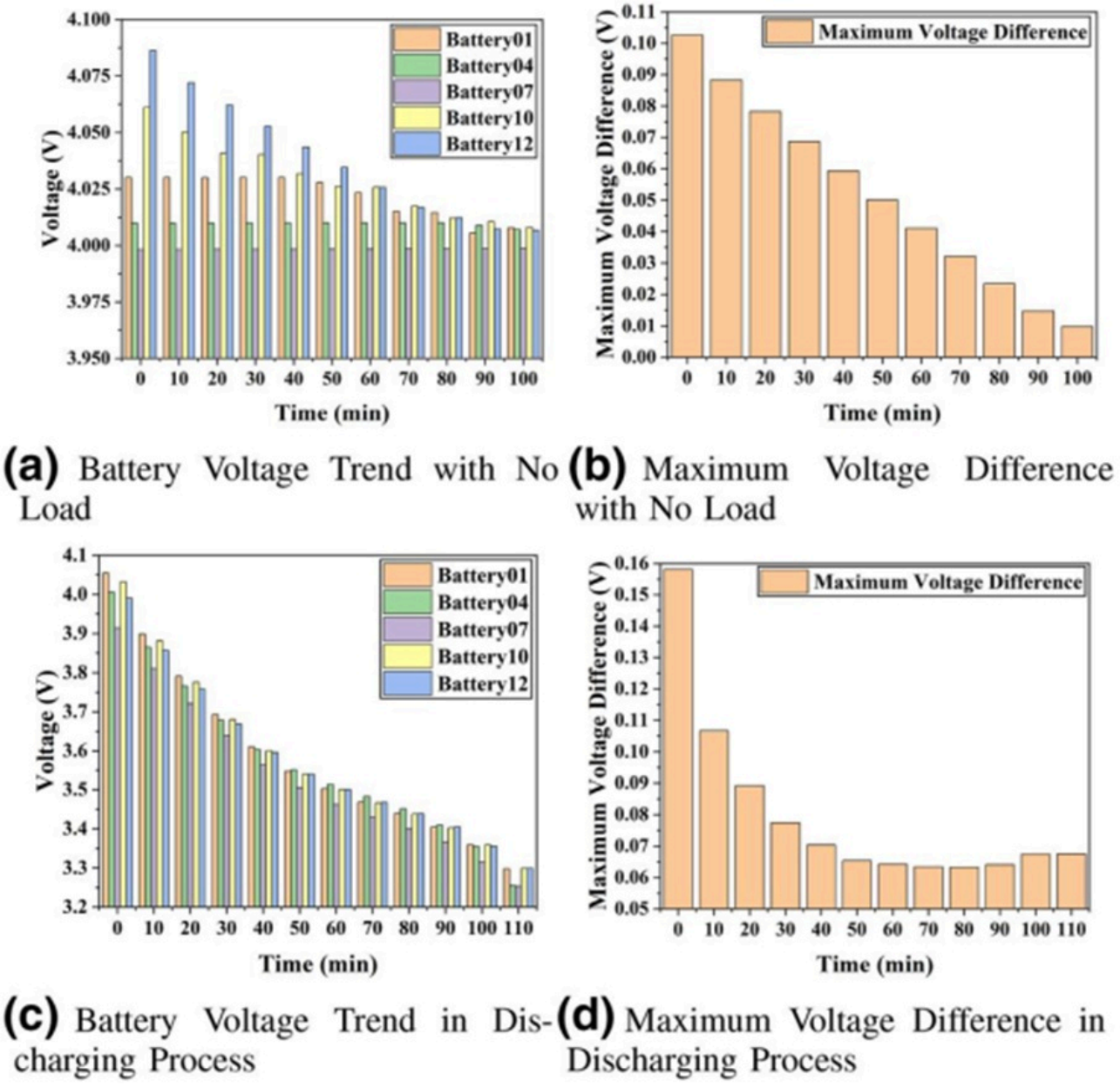

Figure 10. Battery balance test results.

In terms of functional deployment, the computational obligations regarding balance calculations are explicitly delegated to the MCU, whereas the physical execution of the balancing routine is relegated to the SCU. This strict bifurcation of duties dramatically minimizes the intricacies of internal communication protocols and the overall execution of the balancing protocol, substantially bolstering the functional reliability and long-term maintainability of the system.

Local display

To actualize the local display feature, the system selectively apportions specific display responsibilities directly to the MCU and the SCUs. Within this configured environment, the MCU is mandated to present 28 distinct data points, while each SCU is responsible for displaying 62 separate data points. **Figure 11** graphically represents the proportional volume of data transmitted by the MCU relative to the cumulative data traffic, specifically highlighting scenarios involving a

© 2025 The Author(s). | Published by Institute of Smart Energy Systems Press

solitary MCU paired with varying quantities of SCUs. The visual data clearly confirms that once the system architecture incorporates 5 or more SCUs, the data volume broadcast by the MCU drops to less than 10% of the overall total.

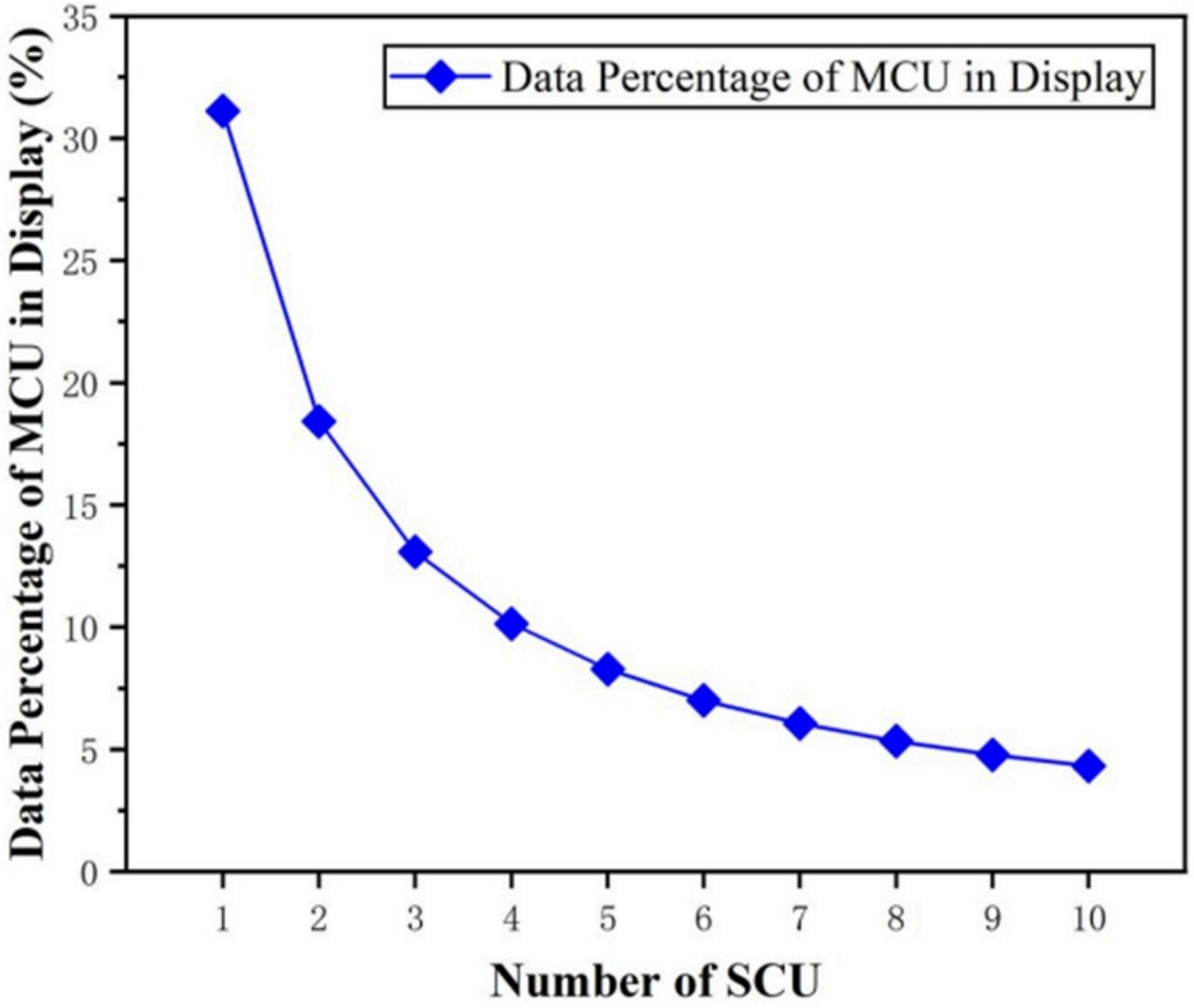

Figure 11. Analysis of local display function.

Employing this specific architectural design ensures a far more logical and efficient distribution of the computational resources housed within both the MCU and the SCUs. This strategic partitioning permits the MCU to dedicate a larger fraction of its processing power toward deeply analyzing and computing vital system status metrics, while simultaneously enabling the SCU to fulfill its designated local operations seamlessly. Ultimately, this well-calibrated distribution of computing assets inherently lowers the baseline performance thresholds required for the central control chips, thereby satisfying critical cost-saving objectives.

Experiments of the multi-parameter optimisation algorithm

Data preparation

The experimental evaluation of the multi-parameter optimization algorithm relies on two distinct traffic network datasets: the Guangzhou traffic network and the Extended Guangzhou traffic network dataset. The standard Guangzhou dataset is acquired utilizing the data collection methodology outlined in ref. [26]. This specific traffic network comprises 50 vertices

© 2025 The Author(s). | Published by Institute of Smart Energy Systems Press

alongside 75 edges, with every edge functioning bidirectionally. Information regarding intersection nodes is extracted via the coordinate selection tool available on Baidu Maps at https://lbsyun.baidu.comp. The charging stations (CSs) are positioned along the network's edges. In total, this network incorporates 20 CSs. **Table 3** details the charging tariffs associated with various charging options across these 20 CSs during different operational periods.

Building upon the foundational Guangzhou dataset, the Extended Guangzhou dataset is generated by applying the same data-gathering approach. This expanded network encompasses 100 vertices, 180 edges, and a total of 45 CSs. **Table 4** presents the charging tariff details for the additional 25 CSs.

Table 3. Energy price table of the Guangzhou dataset

No.	Num of chargers		Energy price (CNY/kWh)					
			Valley		Normal		Peak	
	f	*s*	*f*	*s*	*f*	*s*	*f*	*s*
0	2	3	1.6	1.2	1.8	1.3	1.9	1.5
1	1	2	1.7	1.3	1.9	1.4	2.0	1.6
2	2	3	1.9	1.5	2.1	1.6	2.2	1.8
3	2	4	1.8	1.4	2.0	1.5	2.1	1.7
4	2	5	1.8	1.4	2.0	1.5	2.1	1.7
5	1	2	1.7	1.3	1.9	1.4	2.0	1.6
6	1	3	1.8	1.4	2.0	1.5	2.1	1.7
7	2	1	1.9	1.4	2.0	1.6	2.2	1.7
8	2	3	1.7	1.3	1.9	1.4	2.0	1.6
9	1	2	1.9	1.5	2.1	1.6	2.2	1.8
10	4	6	1.7	1.2	1.8	1.4	2.0	1.5
11	6	4	1.7	1.3	1.9	1.4	2.0	1.6
12	6	5	1.9	1.5	2.1	1.6	2.2	1.8
13	5	3	1.8	1.4	2.0	1.5	2.1	1.7
14	4	2	1.6	1.2	1.8	1.3	1.9	1.5
15	3	2	1.8	1.3	1.9	1.5	2.1	1.6
16	2	7	1.8	1.3	1.9	1.5	2.1	1.6
17	5	2	1.6	1.2	1.8	1.3	1.9	1.5
18	3	4	1.8	1.4	2.0	1.5	2.1	1.7
19	3	5	1.7	1.3	1.9	1.4	2.0	1.6

Table 4. Supplementary energy price table of the Extended Guangzhou data set

© 2025 The Author(s). | Published by Institute of Smart Energy Systems Press

No.	Num of chargers		Energy price (CNY/kWh)					
			Valley		Normal		Peak	
	f	*s*	*f*	*s*	*f*	*s*	*f*	*s*
20	2	4	1.7	1.3	1.9	1.4	2.0	1.6
21	3	3	1.8	1.4	2.0	1.6	2.1	1.7
22	3	4	1.7	1.4	1.9	1.5	2.0	1.6
23	2	5	1.8	1.3	2.0	1.5	2.1	1.6
24	4	5	1.9	1.5	2.0	1.6	2.2	1.8
25	2	3	1.7	1.3	1.9	1.5	2.0	1.6
26	2	4	1.8	1.4	2.0	1.6	2.1	1.7
27	3	3	1.6	1.2	1.8	1.3	1.9	1.5
28	1	3	1.8	1.3	1.9	1.5	2.1	1.6
29	2	2	1.7	1.3	1.9	1.5	2.0	1.6
30	2	4	1.8	1.4	2.0	1.5	2.1	1.7
31	3	2	1.8	1.3	2.0	1.4	2.1	1.6
32	2	5	1.7	1.3	1.9	1.5	2.0	1.6
33	2	6	1.7	1.2	1.9	1.4	2.0	1.5
34	4	4	1.7	1.3	1.9	1.5	2.0	1.6
35	1	3	1.8	1.3	2.0	1.5	2.1	1.6
36	1	2	1.7	1.3	1.8	1.4	2.0	1.5
37	2	3	1.9	1.4	2.0	1.6	2.2	1.7
38	3	4	1.6	1.2	1.8	1.4	1.9	1.5
39	1	3	1.7	1.3	1.9	1.5	2.0	1.6
40	2	5	1.8	1.3	2.0	1.5	2.1	1.6
41	3	4	1.7	1.3	1.9	1.4	2.0	1.6
42	4	5	1.7	1.3	1.9	1.4	2.0	1.6
43	2	4	1.8	1.3	2.0	1.5	2.1	1.6
44	2	3	1.7	1.2	1.9	1.4	2.0	1.5

The scheduling of EV charging operations is executed using time slots as the fundamental unit. **Figure 12** illustrates the segmentation of traffic conditions across 96 time slots within a single day. Notably, the peak traffic periods occur around time slots 34 and 74, respectively.

© 2025 The Author(s). | Published by Institute of Smart Energy Systems Press

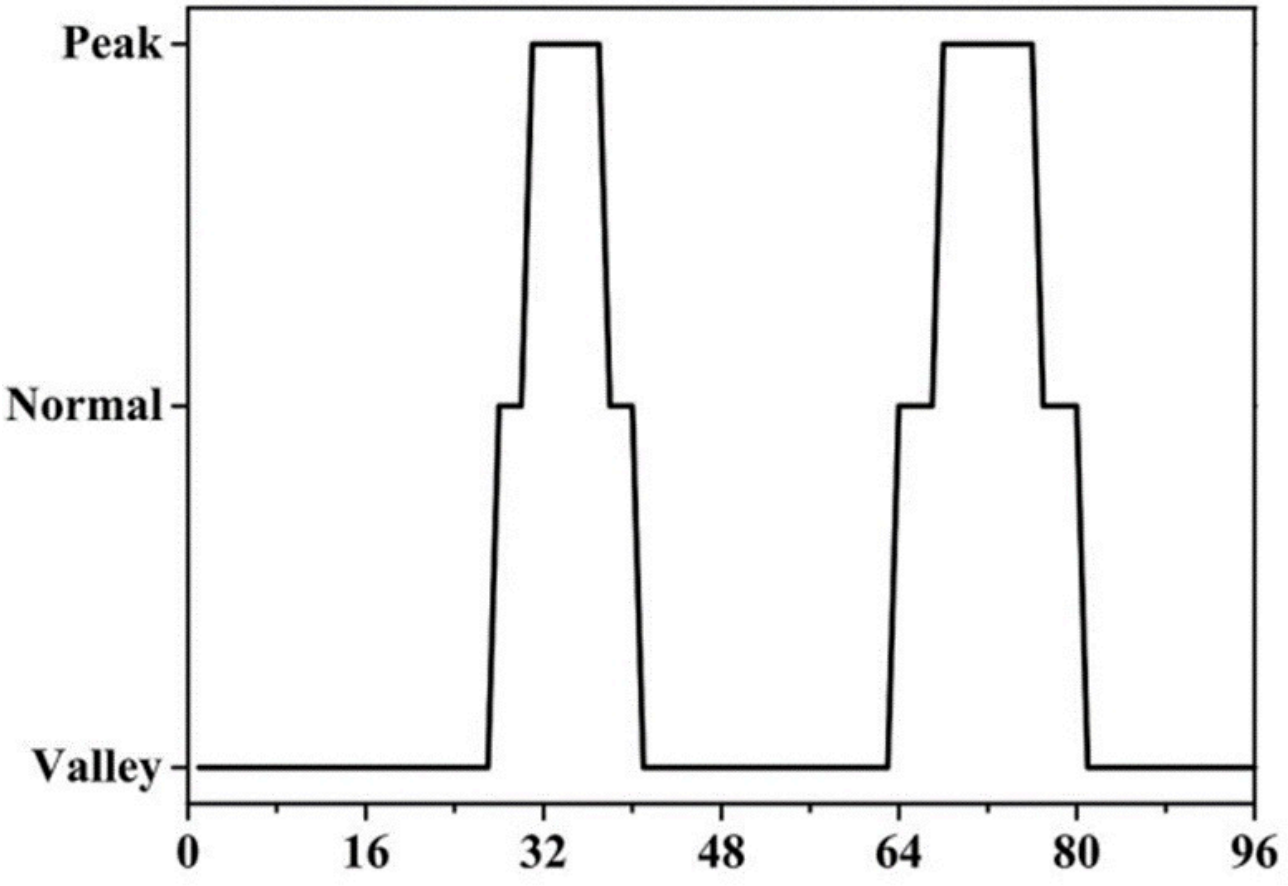

Figure 12. Time slots of one day.

To account for the diverse array of EV models, the vehicle parameters are configured in the following manner: 90% of the fleet possesses a battery capacity of 100 kWh paired with a maximum driving range of 500 km; conversely, the remaining 10% features a 70 kWh battery capacity and a maximum range of 350 km. These two distinct EV profiles align with the long-range and standard configurations of the Tesla Model S, respectively. Both the origin and destination points are chosen at random from the existing vertices within the traffic network. Furthermore, the operational range afforded by the EV's starting battery charge must exceed the spatial distance from its origin to the closest CS. The arrival patterns of the EVs typically follow a Poisson distribution; therefore, a Poisson-distributed random integer is used to simulate EV arrival times before the two identified peak periods. EV travel speeds are assigned randomly among 30 km/h, 40 km/h, and 50 km/h. Based on these specified parameters, a total of 100 and 200 EVs are simulated for the Guangzhou and Extended Guangzhou traffic networks, respectively.

Parameter selection

A parameter selection experiment is executed to determine the optimal variables for the proposed algorithmic framework. Within the previously detailed CS selection operator, the parameter o is evaluated at values of 1, 2, and 3, while various crossover probabilities are tested for the scheduling algorithm, specifically ranging from 0.2 to 0.5.

Across both the parameter selection and comparative trials, all evaluated algorithms achieve the maximum number of charging operations per EV at J = 5, with the target SoC threshold configured to ρ exp = 0.3. Regarding the population-

© 2025 The Author(s). | Published by Institute of Smart Energy Systems Press

based mechanisms, the population size is fixed at N = 30, and the mutation scaling factor is defined as F = 0.5. All of these specific parameters mirror those established in Ref. [26].

The empirical data deployed for the parameter selection trials consists of the Guangzhou dataset alongside its 100 corresponding simulated EVs. A total of twenty independent, repetitive trials are conducted across varying parameter configurations. The previously defined convergence criteria are applied to ascertain the number of iterations required to reach convergence for each parameter set. We systematically evaluate the convergence iteration count, the resulting fitness values, and the variance observed in the average outcome trajectory across these differing combinations. The findings from these parameter selection trials are detailed in **Table 5.**

Table 5. Parameter selection experiment results

C	*o*	Iteration	Fitness	Variance
0.2	1	161	0.2819	0.0032
0.2	2	146	0.3024	0.0172
0.2	3	162	0.2972	0.0085
0.3	1	119	0.2582	0.0017
0.3	2	140	0.2624	0.0020
0.3	3	134	0.2752	0.0043
0.4	1	90	0.2545	0.0034
0.4	2	104	0.2613	0.0033
0.4	**3**	106	0.2572	**0.0016**
0.5	1	**78**	0.2561	0.0022
0.5	2	93	0.2721	0.0047
0.5	3	100	**0.2495**	0.0025

Note: The bold values in the last three columns mean the best results in three aspects, and the bold values in the first two columns mean the parameters finally selected in this paper.

As evidenced by **Table 5**, the iteration count reaches its minimum when C = 0.5 and o = 1. Conversely, configuring C = 0.5 and o = 3 yields the lowest fitness value upon satisfying the convergence criteria. Furthermore, setting C = 4 and o = 3 results in the minimum variance. After a holistic evaluation of these metrics, the parameters are finalized with o set to 3 and the crossover probability C configured to 0.4.

Comparison of experimental results

Both the baseline MVDE algorithm and the newly proposed approach are deployed independently to resolve the EVCS challenge. Within the baseline algorithm, the crossover probability is defined as C = 0.1. Conversely, the proposed methodology utilizes parameters set to o = 3 and C = 0.4. To accurately assess the impact of parameter modifications and the integration of the CS alternative set on algorithmic performance, a modified version of the original MVDE algorithm utilizing C = 0.4 is also included as a benchmark for comparison.

These comparative evaluations utilize the Guangzhou dataset with its 100 simulated EVs, as well as the Extended Guangzhou dataset featuring 200 EVs, as the primary testing data. We evaluate the performance outcomes of the

© 2025 The Author(s). | Published by Institute of Smart Energy Systems Press

baseline algorithm, the modified baseline algorithm (with C = 0.4), and the proposed solution across both designated datasets. For every algorithm and dataset combination, twenty independent and repeated experimental runs are executed to calculate the average performance metrics.

The comparative findings derived from both datasets are presented in **Figures 13 and 14**, respectively.

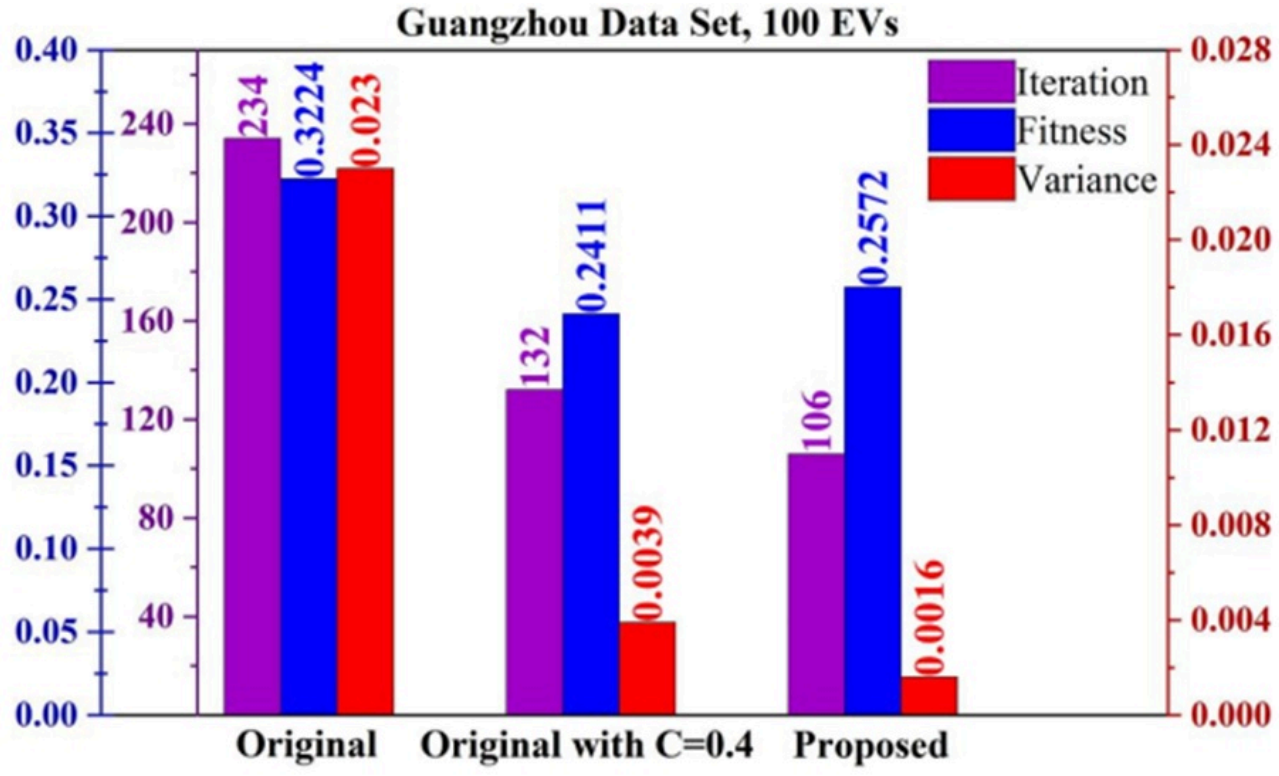

Figure 13. Comparative results of the Guangzhou dataset and 100 EVs.

© 2025 The Author(s). | Published by Institute of Smart Energy Systems Press

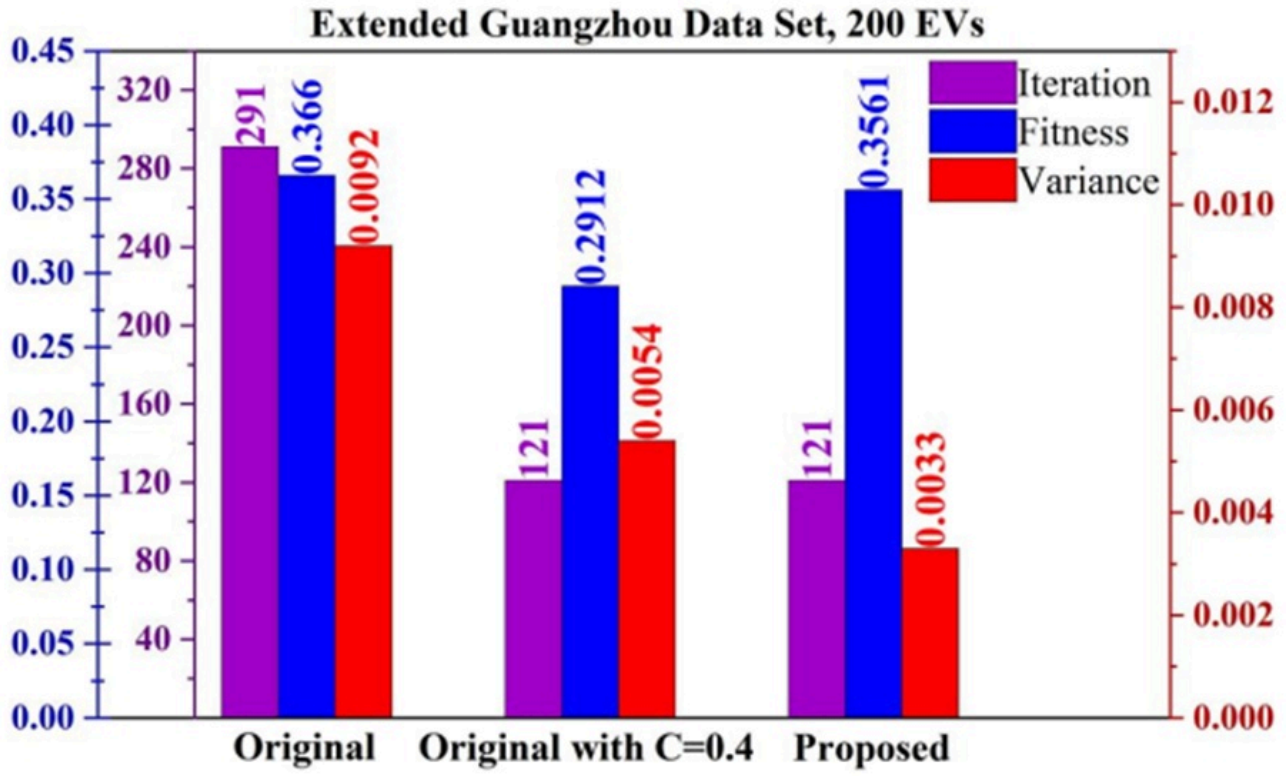

Figure 14. Comparative results of the extended Guangzhou dataset and 200 EVs.

The performance outcomes of the evaluated algorithms across both datasets are scrutinized through three primary lenses: iteration count, fitness value, and overall variance. Regarding iterations, **Figures 13 and 14** clearly demonstrate that both the modified baseline algorithm (C = 0.4) and the proposed approach achieve substantial improvements over the standard baseline algorithm, yielding iteration counts that are closely aligned with one another. This observation implies that the primary driver for reducing iterations is the adjustment of parameter C. Furthermore, the graphical data indicates that the proposed algorithm secures a fitness value that is lower than the standard baseline but higher than the modified baseline (C = 0.4), while simultaneously exhibiting the lowest variance among all three models. Consequently, incorporating the CS alternative set and fine-tuning parameters collectively enhance operational stability.

The final fitness values achieved by both the standard baseline algorithm and the proposed methodology across the two datasets are juxtaposed to analyze variations across three specific dimensions: time, cost, and SoC. As illustrated in **Tables 6 and 7**, the total shift in the optimized fitness value is an aggregate of these three factors. When examined individually, the fluctuation of the fitness value for any single aspect remains variable; it may demonstrate either an increase or a decrease. This variability occurs because the overarching objective of the proposed algorithm is to minimize both the iteration count and the outcome variance, while keeping the cumulative fitness value either reduced or stable. No strict constraints are imposed on the independent directional changes of the three individual fitness components. The algorithm systematically refines the solution to ensure the aggregate fitness value diminishes. If a specific individual aspect exhibits a higher fitness value, it reflects a comprehensive balancing act in which the corresponding fitness values of the other aspects experienced more significant reductions during the optimization process.

Table 6. Comparison of fitness values of the algorithm on the Guangzhou dataset, 100 electric vehicles (EVs)

Algorithm	Fitness	Time	Cost	SoC
Original	0.3224	0.1203	0.1367	0.0654

© 2025 The Author(s). | Published by Institute of Smart Energy Systems Press

Proposed	0.2572	0.1188	0.0994	0.0398
Difference	−0.0652	−0.0015	−0.0373	−0.0256

Table 7. Comparison of fitness values of the algorithm on the Extended Guangzhou data set, 200 electric vehicles (EVs)

Algorithm	Fitness	Time	Cost	SoC
Original	0.3660	0.1479	0.1165	0.1016
Proposed	0.3561	0.1789	0.0797	0.0976
Difference	−0.0099	+0.0310	−0.0368	−0.0040

Through the systematic analysis and comparison of these experimental outcomes, several key conclusions emerge. The algorithm introduced in this study delivers a highly robust optimization outcome by strategically incorporating the CS alternative set and fine-tuning core algorithmic parameters. Compared with the baseline approach, the proposed technique substantially reduces both the required iterations and the statistical variance, while maintaining comparable overall fitness values. Specifically, parameter adjustments serve as the primary catalyst for decreasing the iteration count. Meanwhile, the combined application of the CS alternative set and targeted parameter tuning works synergistically to minimize variance.

Results and Discussion

This manuscript details strategic methodologies designed to assist CS service providers in curtailing operational costs and augmenting revenue streams, specifically through the lenses of robust energy management and optimized EVCS. Regarding energy management, the paper articulates the architectural design and practical implementation of a Battery Management System (BMS) tailored for integration within the Battery Energy Storage System (BESS) of a CS. The designed BMS delivers comprehensive capabilities for continuously monitoring and regulating the operational state of the BESS battery packs. While certain functionalities represent foundational versions, there remains considerable potential for further refinement to elevate the system's overall utility. For instance, integrating machine learning algorithms could enable significantly more precise State of Charge (SoC) estimates.

Additionally, deploying active balancing techniques could further maximize energy efficiency. During BMS operation, it is imperative to calibrate the system parameters precisely in accordance with the specific battery model and inherent characteristics. Furthermore, operators must evaluate the necessity for battery replacement based on both its theoretical lifespan and its real-world performance metrics. Ultimately, the judicious application of a BMS can substantially extend the operational longevity of the batteries.

Addressing the EVCS domain, a novel multi-parameter dynamic scheduling algorithm is introduced, building upon the foundation of existing algorithmic structures. Furthermore, a specific methodology is formulated to evaluate the inherent stability of evolutionary algorithms; this tool is subsequently utilized to assess and compare the stability of both the baseline and the newly proposed algorithms. Compared directly with the baseline model, the dynamic scheduling algorithm presented here achieves accelerated iterative processing and stronger algorithmic stability, while delivering closely comparable optimization results. The computational resolution of this algorithm directly parallels the practical scheduling sequence for EVs. In real-world deployment, this cyclical computational approach can successfully orchestrate EV charging schedules within designated, fixed timeframes. However, a notable limitation of this methodology

© 2025 The Author(s). | Published by Institute of Smart Energy Systems Press

is that, despite iterative speed enhancements, the baseline optimization efficiency inherent to evolutionary algorithms remains somewhat constrained, particularly when confronting massive-scale EVCS challenges. Consequently, practical implementations will necessitate calculated compromises, such as identifying an optimal balance between computation time and the quality of the resulting optimization.

Conclusion

This study delineates two distinct strategies tailored for CS service providers to minimize operational expenditures and boost revenue generation: advanced energy management and optimized EVCS. In the realm of energy management, a sophisticated BMS is engineered and successfully implemented to accommodate large-scale BESS architectures. This BMS executes a variety of essential functions and features targeted enhancements in areas such as interface display and battery balancing. To address the complexities of EVCS, a multi-parameter optimization algorithm is formulated to significantly improve operational practicality. The real-world viability of this scheduling algorithm is rigorously assessed across three specific dimensions: the quality of the optimization effect, the total number of required iterations, and the overall stability. Additionally, a specialized evaluative framework is introduced specifically to quantify the stability of evolutionary algorithms. Ultimately, the empirical findings demonstrate that the integrated BMS proficiently manages battery operations within high-capacity BESS environments, and the newly proposed optimization algorithm offers a marked improvement in practical application compared to preexisting baseline models.

Acknowledgements

None

Conflict of interest

None

Financial support

This work is supported by the Joint Funds of the National Natural Science Foundation of China (U2001204), Tianjin Science Foundation for Distinguished Young Scholars (20JCJQJC00250), Key R&D Program of Tianjin (**20YFZCGX01150**), Tianjin Research Innovation Project for Postgraduate Students (2021YJSB108).

Ethics statement

None

Received: 29 Dec 2023 Revised: 05 Mar 2024 Accepted: 22 Mar 2024
Published online: 15 November 2025

Rights and permissions

Open Access The author(s) retain copyright. This article is licensed under the Creative Commons Attribution-NonCommercial-ShareAlike 4.0 International License. It may be shared and adapted for non-commercial purposes with appropriate attribution, an indication of changes, and distribution of adaptations under the same license. Third-party material may be subject to separate terms identified in its credit line. View the license at https://creativecommons.org/licenses/by-nc-sa/4.0/.

References

1. Moghaddam Z, Ahmad I, Habibi D, Phung QV. Smart charging strategy for electric vehicle charging stations. IEEE Trans Transp Electrific. 2017;4(1):76–88. https://doi.org/10.1109/tte.2017.2753403.

2. Pastor-Fernández C, Bruen T, Widanage WD, Marco J, Gama A. A study of cell-to-cell interactions and degradation in parallel strings: implications for the battery management system. J Power Sources. 2016;329:574–85. https://doi.org/10.1016/j.jpowsour.2016.07.121.

3. Sehil K, Alamri B, Al-Harthi M, Al-Ali A, Al-Mutawa N. Empirical analysis of high voltage battery pack cells for electric racing vehicles. Energies. 2021;14(6):1556. https://doi.org/10.3390/en14061556.

4. Schmuch R, Wagner R, Hörpel G, Placke T, Winter M. Performance and cost of materials for lithium-based rechargeable automotive batteries. Nat Energy. 2018;3(4):267–78. https://doi.org/10.1038/s41560-018-0107-2.

5. Rivera-Barrera JP, Muñoz-Galeano N, Sarmiento-Maldonado HO. SOC estimation for lithium-ion batteries: review and future challenges. Electronics. 2017;6(4):102. https://doi.org/10.3390/electronics6040102.

6. Tian J, Xiong R, Shen W. A review on state of health estimation for lithium ion batteries in photovoltaic systems. eTransportation. 2019;2:100028. https://doi.org/10.1016/j.etran.2019.100028.

7. Zhang F, Hu X, Langari R, Cao D. Hybrid balancing in a modular battery management system for electric-drive vehicles. In: 2017 IEEE Energy Conversion Congress and Exposition (ECCE). IEEE; 2017. p. 578–83.

8. Kıvrak S, Özçelik S, Yılmaz M, Kaya M, Karakaya F. Novel active and passive balancing method-based battery management system design and implementation. J Power Electron. 2021;21(12):1–11. https://doi.org/10.1007/s43236-021-00320-x.

9. Gozdur R, Przerywacz T, Bogdański D. Low power modular battery management system with a wireless communication interface. Energies. 2021;14(19):6320. https://doi.org/10.3390/en14196320.

10. Qiu T, Qiao R, Wu DO. EABS: an event-aware backpressure scheduling scheme for emergency internet of things. IEEE Trans Mob Comput. 2017;17(1):72–84. https://doi.org/10.1109/tmc.2017.2702670.

11. Li W, Rentemeister M, Badeda J, Jöst D, Schulte D, Sauer DU. Digital twin for battery systems: cloud battery management system with online state-of-charge and state-of-health estimation. J Energy Storage. 2020;30:101557. https://doi.org/10.1016/j.est.2020.101557.

12. Qiu T, Qiao R, Wu DO, Chen N, Zhang S. Robustness optimization scheme with multi-population co-evolution for scale-free wireless sensor networks. IEEE/ACM Trans Netw. 2019;27(3):1028–42. https://doi.org/10.1109/tnet.2019.2907243.

13. Chen N, Qiu T, Wu DO, Zhang S, Wang X. An adaptive robustness evolution algorithm with self-competition and its 3D deployment for internet of things. IEEE/ACM Trans Netw. 2021;30(1):368–81. https://doi.org/10.1109/tnet.2021.3113916.

14. Qiu T, Chen N, Zhang S, Wu DO. Born this way: a self-organizing evolution scheme with motif for internet of things robustness. IEEE/ACM Trans Netw. 2022;1–14.

© 2025 The Author(s). | Published by Institute of Smart Energy Systems Press

https://doi.org/10.1109/tnet.2022.3178408.

15. Qiu T, Chen N, Zhang S. Robustness Optimization for IoT Topology. Springer; 2022.

16. Cherukuri M, Kanthi M. Battery management system design for electric vehicle. In: 2019 IEEE International Conference on Distributed Computing, VLSI, Electrical Circuits and Robotics (DISCOVER). IEEE; 2019. p. 1–6.

17. Huang X, Zhang Y, Liu H, Li W, Chen Z. Wireless smart battery management system for electric vehicles. In: 2020 IEEE Energy Conversion Congress and Exposition (ECCE). IEEE; 2020. p. 5620–5.

18. Chen H, Liu Y, Li W, Zhang X, Wang J. Design of a modular battery management system for electric motorcycle. Energies. 2021;14(12):3532.
https://doi.org/10.3390/en14123532.

19. Tarhan B, Yetik O, Karakoc TH. Hybrid battery management system design for electric aircraft. Energy. 2021;234:121227.
https://doi.org/10.1016/j.energy.2021.121227.

20. Wang B, Wang Y, Zhang H, Liu C. Design of lithium battery management system for underwater robot. In: International Conference on Computer Engineering and Networks. Springer; 2020. p. 989–95.

21. Li X, Wang S. A review on energy management, operation control and application methods for grid battery energy storage systems. CSEE J Power Energy Syst. 2019.
https://doi.org/10.17775/cseejpes.2019.00160.

22. Chouhan S, Khaitan SK, Kotecha P, Kulkarni S. DER optimization to determine optimum BESS charge/discharge schedule using linear programming. In: 2016 IEEE Power and Energy Society General Meeting (PESGM). IEEE; 2016. p. 1–5.

23. Junming R, Dai X, Liu J, Chen Y. A novel genetic algorithm-based emergent electric vehicle charging scheduling scheme. In: IECON 2019 - 45th Annual Conference of the IEEE Industrial Electronics Society. Vol. 1. IEEE; 2019. p. 4289–92.

24. Chakraborty N, Mondal A, Mondal S. Intelligent charge scheduling and eco-routing mechanism for electric vehicles: a multi-objective heuristic approach. Sustain Cities Soc. 2021;69:102820.
https://doi.org/10.1016/j.scs.2021.102820.

25. Zhang C, Liu Y, Wu F, Tang B, Wang L. Effective charging planning based on deep reinforcement learning for electric vehicles. IEEE Trans Intell Transp Syst. 2020;22(1):542–54.
https://doi.org/10.1109/tits.2020.3002271.

26. Liu W-L, Lin Y, Liu S, Chen Y, Zhou M. Coordinated charging scheduling of electric vehicles: a mixed-variable differential evolution approach. IEEE Trans Intell Transp Syst. 2019;21(12):5094–109.
https://doi.org/10.1109/tits.2019.2948596.

27. Hu D, Li X, Wang Y, Zhang L, Chen Q. Research and design of retired power battery management system applied to communication base station. In: 2020 Chinese Automation Congress (CAC). IEEE; 2020. p. 2761–5.

28. Yang S-N, Cheng W-S, Hsu Y-C, Gan C-H, Lin Y-B. Charge scheduling of electric vehicles in highways. Math Comput Model. 2013;57(11-12):2873–82.
https://doi.org/10.1016/j.mcm.2011.11.054.

29. Chen T, Zhang B, Pourbabak H, Kavousi-Fard A, Su W. Optimal routing and charging of an electric vehicle fleet for high-efficiency dynamic transit systems. IEEE Trans Smart Grid. 2016;9(4):3563–72.
https://doi.org/10.1109/tsg.2016.2635025.

30. Triviño-Cabrera A, Aguado JA, de la Torre S. Joint routing and scheduling for electric vehicles in smart grids with V2G. Energy. 2019;175:113–22.

© 2025 The Author(s). | Published by Institute of Smart Energy Systems Press

https://doi.org/10.1016/j.energy.2019.02.184.

31. Wang G-G, Gao D, Pedrycz W. Solving multi-objective fuzzy job-shop scheduling problem by a hybrid adaptive differential evolution algorithm. IEEE Trans Ind Inf. 2022;18(12):8519–28. https://doi.org/10.1109/tii.2022.3165636.

32. Zhang Z, Wang G-G, Li Y, Chen X, Zhao L. An efficient interval many-objective evolutionary algorithm for cloud task scheduling problem under uncertainty. Inf Sci. 2022;583:56–72. https://doi.org/10.1016/j.ins.2021.11.027.

33. Wu X, Cao Z. An improved multi-objective evolutionary algorithm based on decomposition for solving re-entrant hybrid flow shop scheduling problem with batch processing machines. Comput Ind Eng. 2022;169:108236. https://doi.org/10.1016/j.cie.2022.108236.

34. Storn R, Price K. Differential evolution – a simple and efficient heuristic for global optimization over continuous spaces. J Glob Optim. 1997;11(4):341–59. https://doi.org/10.1023/a:1008202821328.

35. Lin Y, Liu W-L, Zhou M, Chen Y, Li X. A hybrid differential evolution algorithm for mixed-variable optimization problems. Inf Sci. 2018;466:170–88. https://doi.org/10.1016/j.ins.2018.07.035.

36. Zhao W, Beach TH, Rezgui Y. A systematic mixed-integer differential evolution approach for water network operational optimization. Proc R Soc A Math Phys Eng Sci. 2018;474(2217):20170879. https://doi.org/10.1098/rspa.2017.0879.

37. Chen Z, Liu Y. Individuals redistribution based on differential evolution for covariance matrix adaptation evolution strategy. Sci Rep. 2022;12(1):1–16. https://doi.org/10.1038/s41598-021-04549-1.

38. Kushwah GS, Ranga V. Detecting DDoS attacks in cloud computing using extreme learning machine and adaptive differential evolution. Wirel Pers Commun. 2022;124(3):1–24. https://doi.org/10.1007/s11277-022-09481-9.

© 2025 The Author(s). | Published by Institute of Smart Energy Systems Press